International Journal of Greenhouse Gas Control 14 (2013) 151–168

Contents lists available at SciVerse ScienceDirect

International Journal of Greenhouse Gas Control

journal homepage: www.elsevier.com/locate/ijggc

Hydrogeochemistry of surface and spring waters in the surroundings of the CO_2 injection site at Hontomín–Huermeces (Burgos, Spain)

Barbara Nisi[a,*], Orlando Vaselli[b,c], Franco Tassi[b,c], Javier de Elio[d,e], António Delgado Huertas[f], Luis Felipe Mazadiego[d], Marcelo F. Ortega[d]

[a] CNR-IGG Institute of Geosciences and Earth Resources, Via Moruzzi 1, 56124 Pisa, Italy
[b] Department of Earth Sciences, Via G. La Pira 4, 50121 Florence, Italy
[c] CNR-IGG Institute of Geosciences and Earth Resources, Via G. La Pira 4, 50121 Florence, Italy
[d] ETS Ingenieros de Minas Universidad Politécnica de Madrid, Calle de Ríos Rosas 21, 28003 Madrid, Spain
[e] Ciudad de la Energia, II Av. de Compostilla 2, 24400 Ponferrada, Leon, Spain
[f] Instituto Andaluz de Ciencias de la Tierra IACT(CSIC-UGR), Avda. de las Palmeras 4, 18100 Armilla, Granada, Spain

ARTICLE INFO

Article history:
Received 10 March 2012
Received in revised form 8 December 2012
Accepted 8 January 2013
Available online 9 February 2013

Keywords:
Hontomín–Huermeces
CO_2 injection
Geochemical monitoring
Dissolved gases
Trace elements
Carbon isotopes

ABSTRACT

In this paper the very first geochemical and isotopic data related to surface and spring waters and dissolved gases in the area of Hontomín–Huermeces (Burgos, Spain) are presented and discussed. Hontomín–Huermeces has been selected as a pilot site for the injection of pure (>99%) CO_2. Injection and monitoring wells are planned to be drilled close to 6 oil wells completed in the 1980s for which detailed stratigraphical logs are available, indicating the presence of a confined saline aquifer at the depth of about 1500 m into which less than 100,000 tons of liquid CO_2 will be injected, possibly starting in 2013.

The chemical and features of the spring waters suggest that they are related to a shallow hydrogeological system as the concentration of the Total Dissolved Solids approaches 800 mg/L with a $Ca^{2+}(Mg^{2+})$-HCO_3^- composition, similar to that of the surface waters. This is also supported by the oxygen and hydrogen isotopic ratios that have values lying between those of the Global and the Mediterranean Meteoric Water Lines. Some spring waters close to the oil wells are characterized by relatively high concentrations of NO_3^- (up to 123 mg/L), unequivocally suggesting an anthropogenic source that adds to the main water–rock interaction processes. The latter can be referred to Ca-Mg-carbonate and, at a minor extent, Al-silicate dissolution, being the outcropping sedimentary rocks characterized by Palaeozoic to Quaternary rocks. Anomalous concentrations of Cl^-, SO_4^{2-}, As, B and Ba were measured in two springs discharging a few hundred meters from the oil wells and in the Rio Ubierna. These contents are significantly higher than those of the whole set of the studied waters and are possibly indicative of mixing processes, although at very low extent, between deep and shallow aquifers. No evidence of deep-seated gases interacting with the Hontomín–Huermeces waters was recognized in the chemistry of the dissolved gases. This is likely due to the fact that they are mainly characterized by an atmospheric source as highlighted by the high contents of N_2, O_2 and Ar and by N_2/Ar ratios that approach that of ASW (Air Saturated Water) and possibly masking any contribution related to a deep source. Nevertheless, significant concentrations (up to 63% by vol.) of isotopically negative CO_2 (<−17.7‰ V-PDB) were found in some water samples, likely related to a biogenic source.

The geochemical and isotopic data of this work are of particular importance when a monitoring program will be established to verify whether CO_2 leakages, induced by the injection of this greenhouse gas, may be affecting the quality of the waters in the shallow hydrological circuits at Hontomín–Huermeces. In this respect, carbonate chemistry, the isotopic carbon of dissolved CO_2 and TDIC (Total Dissolved Inorganic Carbon) and selected trace elements can be considered as useful parameters to trace the migration of the injected CO_2 into near-surface environments.

* Corresponding author. Tel.: +39 050 3152320; fax: +39 050 3152323.
E-mail addresses: b.nisi@igg.cnr.it, barbara.nisi@unifi.it (B. Nisi).

1750-5836/$ – see front matter © 2013 Elsevier Ltd. All rights reserved.
http://dx.doi.org/10.1016/j.ijggc.2013.01.012

1. Introduction

The Hontomín–Huermeces (hereafter HH) area (Fig. 1) is located at about 30 km north of Burgos (Spain) and lies in the north-central region of the Iberian Peninsula, where the NE sector of the Duero Basin is bordered by the Basque-Cantabrian Range to the north and by the Iberian Range to the southeast. The Basque-Cantabrian Basin is considered one of the most prospective sedimentary basins in Spain in terms of hydrocarbon exploration (Quesada et al., 1997; Permanyer et al., 2013), due to the presence of a large variety of source rocks, reservoirs and seals and abundant structural and stratigraphic traps. In the surrounding areas of the target site, oil and gas production were carried out onshore (Ayoluengo oil, discovered 1964, and Castillo gas fields) and offshore (Gaviota and Albatros gas fields). Moreover, non-commercial oil discoveries are reported in several zones, e.g. Huidobro, Tozo and Hontomín structures (e.g. Quesada et al., 1993, 1995, 1997; Quesada and Robles, 1995).

The HH area was selected as a site to establish a scientific plant for CO_2 capture and storage (Lupion et al., 2011). A multidisciplinary (geophysics, structural geology, hydrogeology and geochemistry) approach, funded by the Spanish Government and the European Community through a state-owned Foundation (Ciudad de la Energia), is presently carried out to demonstrate that CCS (Carbon Capture and Storage) is feasible and can be considered one of the most suitable techniques to reduce the emission of anthropogenic greenhouse gases.

Six wells (namely Hontomín-1 to Hontomín-4, Hontomín SW1 and Montorio-1), drilled in HH for oil exploration (Fig. 1), are an important source for geological and structural information of both the aquifer-bearing horizon where the injection of CO_2 will be occurring and the cap rock. Once injected underground, CO_2 can be retained at depth (Gunter et al., 1993, 2000, 2004), as: (a) supercritical fluid (physical trapping), (b) fluid migrating very slowly in an aquifer (hydrodynamic trapping), (c) dissolved $CO_{2(aq)}$ into reservoir water (solubility trapping), and (d) newly formed carbonates (mineral trapping) (e.g. Cantucci et al., 2009 and references therein). Among these sequestration processes, mineral trapping is likely the most stable (e.g. Gunter et al., 1993, 1997). The injection of CO_2 in oil, gas and coal-bed methane fields can be used to recover methane and other hydrocarbons (Carbon Sequestration with Enhanced Gas Recovery and Oil Recovery: CSEGR and CSEOR, respectively, referred collectively as CO_2-EHR, e.g. Oldenburg, 2003; Solomon et al., 2008), representing an economic advantage that can partly decrease the costs of the CO_2 storage underground. Risks of CO_2 leakage and seepage from the reservoir to the surface need to be carefully evaluated (e.g. Pruess and García, 2002; Rutqvist and Tsang, 2002; Damen et al., 2006; Jones et al., 2006; Voltattorni et al., 2006; Cantucci et al., 2009). Detection of escaped CO_2 is a challenge since the release of the stored CO_2 may occur shortly after the injection or be delayed for few to thousands years.

The presence of CO_2 plume in an aquifer-bearing geological formation requires geophysical and geochemical monitoring programs to understand the fate of injected CO_2 in terms of safety and verification purposes. CO_2 storage monitoring programs are also addressed to demonstrate whether CO_2 storage projects are effective in reducing atmospheric levels of CO_2 by both predicting the fate of the stored carbon dioxide and recognizing leakages to the environment (e.g. IPCC, 2005; Korre et al., 2011). In this respect geochemical investigation plays a key role in detecting CO_2 leakages from the reservoir since if they occur migration into the shallow groundwater systems, through the topsoil and then into the atmosphere might be expected.

CCS pilot sites, such as that at HH, are also aimed to test that this technique is a viable option for CO_2 mitigation and allow to define the most adequate physical and chemical monitoring methodologies to prove the reliability of CO_2 storage at depth. Nevertheless, the definition of the chemical and isotopic background of the water discharges is the correct approach before a carbon dioxide injection and is useful for the subsequent intra- and post-injection geochemical monitoring programs.

A pre-injection geochemical survey of natural water discharges is thus mandatory in order to establish whether their chemical and isotopic features can be modified when CO_2 leaks are interfering with the shallow waters. Consequently, this paper reports a detailed geochemical and isotopic study in the HH area with the aim to: (i) provide a geochemical characterization of the surface and spring water discharges,(ii) assess the main geochemical processes that affect the shallow hydrogeological system, (iii) propose a geochemical approach to ascertain the origin of CO_2 in the dissolved gases prior the injection and (iv) suggest which geochemical and isotopic parameters can be regarded as suitable tracers of CO_2 leakages at the near-surface.

2. Geological and hydrogeological setting

2.1. Geological outlines

Palaeozoic metasediments are the oldest geological formations recorded in the HH area and are discordantly overlain by the Alpine cycle, which consists of Triassic (lime- and dolostones and evaporites), Jurassic (lime- and dolostones and marls) and Cretaceous (turbidites, conglomerates, shale and lime- and dolostones) formations (Fig. 1). Sanchez-Moya and Sopena (2004) suggested that these sediments are associated with the rifting process occurring during the closure of the Tethys and the opening of the Atlantic Ocean. In the Cretaceous-Paleogene, the very first compressive movements of the Alpine orogeny occurred, producing the onset of the formation of the Duero Basin. The climax of the deformation took place in the Oligocene-Lower Miocene, when the sedimentation of the synorogenic complex was underway (Santisteban et al., 1996). The Neogene sedimentation produced fluvial deposits, mainly located in the western margin and alluvial fan systems close to the active northern and eastern margins in the Duero Basin (Mediavilla et al., 1996). In the north-eastern region of the Duero Basin the sequence consists of Lower Miocene marls, clays, evaporitic and limestone deposits. In the Middle Miocene the emplacement of alluvial facies along the north and north-east margins of the Duero Basin occurred. A limestone layer closes the sequence (Mediavilla et al., 1996) and is topped by lacustrine sediments of Middle-Upper Miocene age. The Pliocene-Pleistocene sedimentation includes alluvial fan gravels. Quaternary deposits consist of gravels, sands, silts and clays.

From a structural point of view, this region corresponds to the Cenozoic basins (NE Duero and Bureba Depression) and the Alpine orogenic system (Iberian and Basque-Cantabria Ranges). The Basque-Cantabrian Range is the eastern extension of the Pyrenean system and refers to the compressive tectonics that has produced displacement of the Cantabrian Sea crust under the Iberian plate (Hernaiz et al., 1994; Tavani and Anton Muñoz, 2012; Tavani et al., 2011). The Iberian Range forms a NW-SE striking intraplate fold belt (Benito-Calvo and Perez-Gonzalez, 2007 and references therein), which started with the Mesozoic extensional stages, whereas the compressive phase occurred in the Cretaceous. The studied area includes the westernmost part of the Paleozoic Sierra de la Demanda and a zone of Mesozoic materials structured in NW-SE/WNW-ESE anticlines and synclines (Benito-Calvo and Perez-Gonzalez, 2007 and references therein). The outcropping Mesozoic rocks of the Sierra de Atapuerca are located in the Neogene basins between the two ranges. With the exception of the fold and fracture systems affecting the Paleogene deposits, the

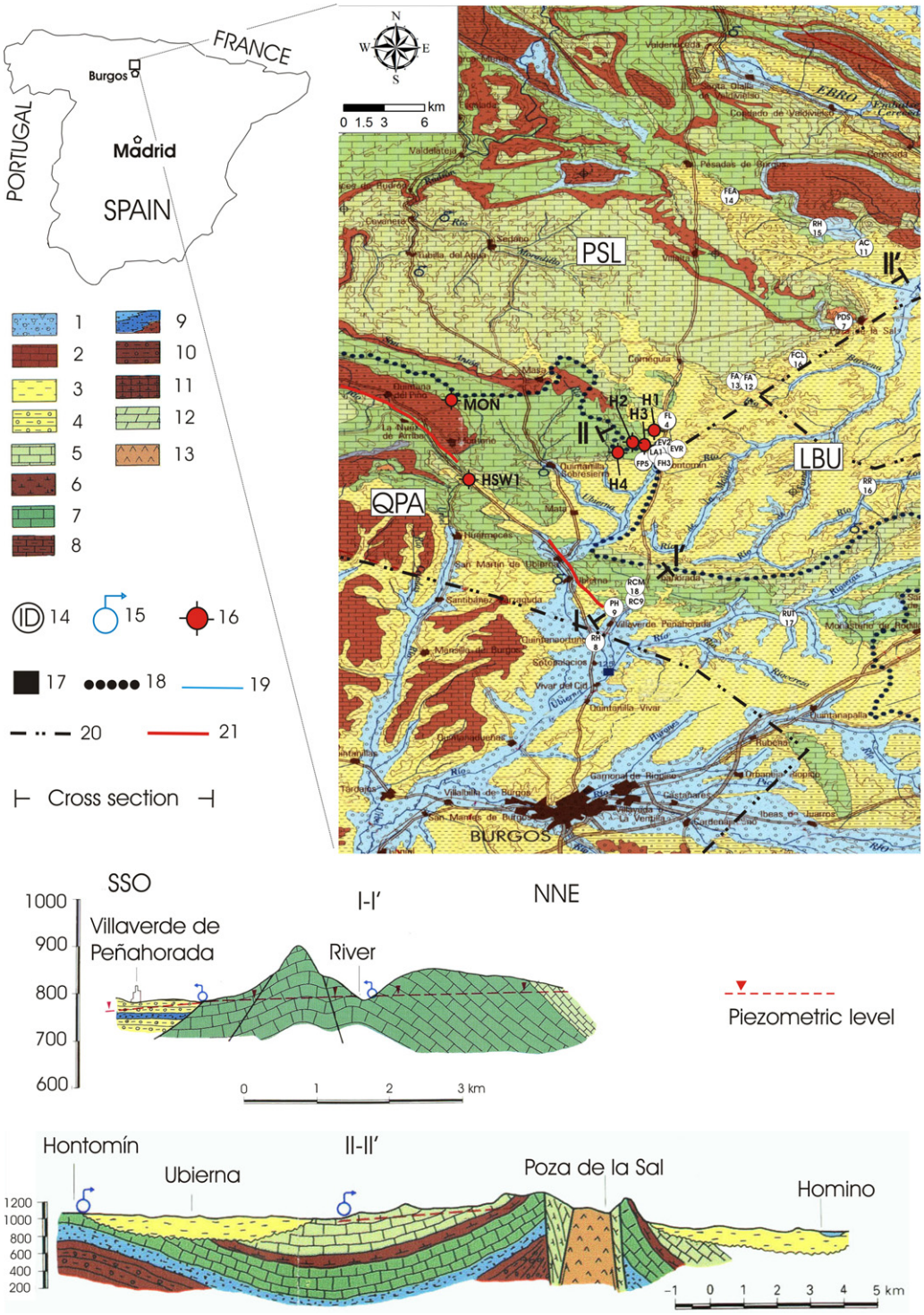

Fig. 1. Schematic geological map of the Hontomín–Huermeces area. 1. Quaternary deposits (gravels, sands, silts and clay); 2. Pliocene formations (limestone and marls); 3. Eocene-Miocene formations (marls, clay, limestone and gypsum, and conglomerates); 4. Eocene-Miocene formations (turbidites, conglomerates, lutites and clay); 5. Upper Cretaceous formations (bioclastic calcareous sandstones); 6. Upper Cretaceous formations (marls, marly limestones); 7. Upper Cretaceous formations (limestones, calcareous sandstones); 8. Upper Cretaceous formations (clay limestones and marls); 9. Lower Cretaceous formations (sands and silts); 10. Lower Cretaceous formations (clay-rich sandstones, conglomerates and limestones); 11. Upper Lias formations (calizas arcillosas and marls); 12. Jurassic Lias formations (limestones, dolostone, marls and carniola); 13. Upper Triassic formations (F. Keuper: clays and gypsum); 14. Sampling sites; 15. Creeks; 16. Oil wells (H1: Hontomín-1; H2: Hontomín-2; H3: Hontomín-3; H4: Hontomín-4; HSW1: Hontomín-SW1; MON: Montorio); 17. Villages and cities; 18. Hydrographic limits of the Duero and Ebro basins; 19. Rivers; 20. Limits of the different hydrographic units (QPA: Quintanilla-Peñahorada-Atapuerca; PSL: Pàramos de Sedano-La Lora; LBU: La Bureba); 21. Ubierna fault.

Source: Modified after ITGE (1998).

general trend in the Cenozoic basins is the occurrence of Neogene (sub)horizontal sediments (Hernaiz et al., 1994).

2.2. Hydrogeological feature

The HH area is located between the hydrographic catchments of the Duero and Ebro rivers in a typical continental Mediterranean climate regime, with an annual rainfall pattern characterized by two peaks of precipitation, in autumn and spring, respectively. Mean annual rainfall values range from 650 mm, mainly in the low lands, up to 800 mm in the mountainous areas (Agencia Estatal de Meteorologia; AEMET, www.aemet.es).

The main tributaries characterized by a permanent hydrographic regime are the Arlanzon River (not shown in Fig. 1) and its tributaries (Urbel and Ubierna) and the Oca and Rudron rivers (not shown in Fig. 1) for the Duero and Ebro basins, respectively. In the western slope of the Ebro basin the Homino River flows through the central part of the studied area up to Hontomin village (Fig. 1). According to ITGE (1998), the main drainage network at HH is characterized by the prevalence of three hydrogeological units, as follows: (i) "Quintanilla-Peñahorada-Atapuerca" (SW of HH), belonging to the Duero hydrographic catchment, (ii) "Pàramos de Sedano-La Lora" (NW of HH) and (iii) "La Bureba" (SE of HH), related to the Ebro hydrographic basin (Fig. 1). Ultimately, Tertiary detritic materials of low permeability fill the Ebro and Duero basins.

The "Quintanilla-Peñahorada-Atapuerca" (QPA) hydrogeological unit mainly consists of Cretaceous sedimentary formations and is placed in the southern part overboard of the studied area. This unit includes tectonized calcareous formations and the recharge is mainly via direct infiltration of the rainfalls, and groundwater feeding the superficial diffuse drainages, where low permeability lithologies occur. The WNW-ESE oriented Ubierna fault (partially masked by Tertiary units), crossing the Mesozoic series, is considered to be responsible for the ascent of the Upper Triassic plastic formations (Keuper Formation) (e.g. Hernaiz, 1994; Tavani et al., 2011; Quintá and Tavani, 2012). Consequently, waters circulating inside the Jurassic and Lower Cretaceous formations, located to the North with respect to the Ubierna fault, have generally a NE direction, whereas waters circulating in the southern sector are influenced by a saline domo-shape structure and have generally a preferential flow path in sub-parallel direction.

The "Pàramos de Sedano-La Lora" (PSL) hydrogeological unit is entirely located in the western sector of the studied area, between the Ebro River and the hydrographic limits of the Duero basin and covers the north-western area of the geological structural of the CO_2 injection pilot site. The hydrogeological units are mainly represented by karstic calcareous formations and by the Utrillas formation mainly consisting of fluvial sands (Arostegui et al., 2000).

Finally, the "La Bureba" (LBU) hydrogeological unit occupies the southern part of the area under study. This unit is situated between the hydrographic limits of the Duero and Ebro basins and the Burgos region. The main hydrogeological unit is represented by carbonate sequences. Most recharge is directly derived by infiltration of the rainfalls through permeable outcrops and into the Tertiary facies (sands and conglomerates). Carbonates formations maintain continuity with respect to the PSL hydrogeological units. This implies that PSL may receive contributions from "La Bureba" hydrogeological unit.

The geological setting of the pilot test site for the CO_2 injection is located in a dome-shape structure affecting the Lower Jurassic formations (Alcalde et al., 2010). The CO_2-hosting reservoir is a saline aquifer at the depth of about 1500 m in a calcite-dolomite rich level of Sinemurian age. The lower and upper sealing formations consist of anhydritic unit (Keuper Formation) and marls of Pliensbachian age, respectively. The geological reservoir is in agreement with the EU recommendations, assessing that a CO_2 trap has to be characterized by a thickness of 20–50 m, a porosity of 10% or less, a cap-rock (Lower Jurassic marls) thickness of 50–100 m and a water salinity >10 g/L. At the surface the injection well (close to which a monitoring well is planned to be drilled) will be located between Hontomín-2 and Hontomín-4 oil wells (Fig. 1).

3. Materials and methods

Five sampling campaigns (January, July and November 2010 and March and April 2011) were carried out in the surroundings of HH areas up to a distance of about 20 km with respect to the site where the CO_2 injection well is planned. In total, 19 surface (RU8, RC9, RH15, RR16, RUT17, RCM18) and spring (LA1, EV2, FH3, FL4, FP5, FCL6, PDS7, PH9, AC11, FA12, FA13, FEA14, EVR) waters were collected (Fig. 1). Some springs (namely, LA1, EV2, FH3, FL4, FP5) were repeatedly sampled in all the campaigns, since they are discharging close to the injection site. Other waters, e.g. FCL6, PDS7, PH9, AC11, sampled in July and November 2010 and March 2011 (Table 1), are mostly distributed between the Ubierna Fault to the SW and the Triassic salt dome structure to the NE (Serrano-Oñate et al., 1990). These springs are related to either the contact between impervious and permeable formations or overflow discharges (Fig. 1). To the best of our knowledge, no domestic or industrial wells are present in the studied area.

Temperature and pH were measured in the field by means of portable instruments. Total alkalinity was determined in the field by acidimetric titration using HCl 0.01N as titrating agent and methyl-orange as indicator. Two water aliquots were collected for the determination of: (a) anions and (b) cations and trace elements. The latter was acidified by adding Suprapur nitric acid (1% HNO_3). Both aliquots were filtered at 0.45 μm in the field. About 50 mL of water were sampled for the determination of free-CO_2 in pre-weighed glass bottles into which 5 mL of 1 M Na_2CO_3 were added. "Free-CO_2" refers to CO_2 present in water as both gas microbubbles (CO_{2gas}) and dissolved phase (CO_{2liq}), the latter being CO_2 not yet transformed into HCO_3^-. Consequently, free-CO_2 is a useful parameter to detect "active" CO_2 inputs in aquifers. An aliquot of 125 mL of water was sampled for the isotopic analysis of oxygen and hydrogen (January and November 2010) in H_2O and carbon (January 2010) in TDIC (Total Dissolved Inorganic Carbon), after adding few milligrams of $HgCl_2$ to inhibit carbon isotopic fractionation by bacteria. The sampling for the determination of the dissolved gases and carbon isotopes ($^{13}C/^{12}C$) in CO_2 was carried out by using 250 mL pre-evacuated glass bottles equipped with Torion® stopcocks (Tassi et al., 2004, 2008, 2009). In the laboratory the gas vials are pre-evacuated by a rotary pump to a vacuum of 10^{-1}–10^{-2} Pa. By immerging the gas vial into the water and opening the Teflon stopcock, the water is forced to enter the vial by decompression; about 2/3 of the glass bottles were filled with water.

Water samples were analyzed by ion chromatography (Cl^-, SO_4^{2-}, NO_3^-, Br^-, and F^-), molecular spectrophotometry (NH_4), atomic absorption spectrophotometry (Na^+, K^+, Ca^{2+}, and Mg^{2+}), and inductively coupled plasma-mass spectrometer (Al, As, B, Ba, Cd, Co, Cr, Cs, Cu, Fe, Li, Mn, Ni, P, Pb, Rb, Sb, Se, Si, Sr, Tl, U, V, W and Zn). Errors were <3% for the main components and 10–15% for trace elements.

The concentration of free-CO_2 was calculated on the basis of the analysis of total alkalinity after potentiometry titration with a 0.5 M HCl solution. The isotopic composition of oxygen and hydrogen in H_2O (expressed as $\delta^{18}O$ and δ^2H‰ V-SMOW, respectively) was analyzed by using a Finningan Delta Plus XL mass spectrometer. Water samples were equilibrated with CO_2 for the analysis of $\delta^{18}O$ values (Epstein and Mayeda, 1953), while the hydrogen isotopic ratios were measured on H_2 produced by the reaction of 10 μL of water with metallic zinc at 500 °C, following the analytical

Table 1
Location, sampling date, geographical coordinates, temperature (°C), pH and chemical composition of the HH waters.

Sample	Locality	type	Date	Est	North	Temp.	pH	Na	K	Ca	Mg	HCO_3	Cl	SO_4	F	Br	NO_3	NH_4	Σcat	Σan	Err. %	TDS	Free CO_2
LA1	Laguillo	spring	jan-2010	446898	4714368	10.9	7.2	11.0	0.8	97	3.5	265	8.0	16.0	0.02	0.03	76.0	n.d.	5.64	6.13	-4.19	493	n.d.
EV2	El Vivero	spring	jan-2010	447840	4714727	11.6	7.4	3.1	0.9	88	4.3	289	3.3	4.9	0.05	0.02	14.0	0.04	4.91	5.16	-2.43	408	n.d.
FH3	Fuente de Hontomin	spring	jan-2010	447725	4736410	9.5	7.3	20.0	4.7	140	8.2	332	30.0	50.0	0.06	0.08	69.0	0.12	8.67	8.45	1.32	636	n.d.
FL4	Fuente Lordujo	spring	jan-2010	448000	4716626	7.6	7.8	2.1	0.4	83	4.9	249	8.9	16.0	0.40	0.03	16.0	0.05	4.66	4.93	-2.79	381	n.d.
FP5	Fuente Peña	spring	jan-2010	446694	4713593	11.2	7.1	2.8	1.3	91	5.4	270	8.2	12.0	0.35	0.03	26.0	0.06	5.15	5.33	-1.67	417	n.d.
LA1	Laguillo	spring	jul-2010	447436	4714124	13.5	7.7	12.7	0.9	105	1.5	283	7.4	9.7	n.d.	<0.01	30.0	0.03	5.95	5.53	3.62	451	0.934
EV2	El Vivero	spring	jul-2010	447840	4714727	11.5	7.3	3.8	1.2	94	2.0	279	2.0	3.5	0.05	0.02	9.1	0.03	5.06	4.85	2.14	395	1.136
FH3	Fuente de Hontomin	spring	jul-2010	447725	4736410	12.8	7.2	34.0	4.6	155	5.2	383	29.0	66.0	0.21	0.03	65.0	0.04	9.78	9.52	1.32	742	0.301
FL4	Fuente Lordujo	spring	jul-2010	448000	4716626	10.5	7.6	2.6	0.5	98	2.5	272	6.7	12.0	0.47	0.03	14.0	0.03	5.23	5.12	1.05	409	0.560
FP5	Fuente Peña	spring	jul-2010	446694	4713593	13.0	7.4	3.3	1.1	104	2.5	282	5.1	11.0	0.50	0.03	23.0	0.04	5.58	5.37	1.94	433	1.167
FCL6	Fuente Castil de Lences	spring	jul-2010	455206	4721182	14.0	7.4	2.4	0.6	76	6.7	259	2.2	2.1	0.02	0.05	5.5	0.03	4.47	4.44	0.36	355	0.076
PDS7	Fuente Poza De La Sal	spring	jul-2010	457740	4723975	10.5	7.5	3.7	0.5	64	7.0	220	6.5	7.2	0.41	0.02	0.9	0.05	3.95	3.95	-0.03	310	0.565
RU8	Rio Ubierna	river	jul-2010	443957	4700205	17.0	8.0	11.7	1.5	90	8.0	274	10.0	21.0	0.37	0.04	7.1	0.06	5.71	5.33	3.46	424	0.748
PH9	Fuente Peñahorada	spring	jul-2010	446963	4705202	12.0	7.4	3.0	0.6	82	5.5	266	3.4	5.2	0.18	0.05	8.9	0.02	4.70	4.71	-0.10	375	n.d.
RC9	Rio Cantera	spring	jul-2010	446149	4703341	19.0	8.2	8.6	1.0	90	5.2	315	9.9	7.3	0.73	<0.01	4.3	0.05	5.33	5.67	-3.05	442	0.727
AC11	Aguas Candidas	spring	jul-2010	458895	4729421	10.5	7.4	2.8	0.7	89	6.2	274	3.8	5.1	0.55	0.03	3.7	0.03	5.10	4.77	3.41	386	n.d.
FA12	Fuentona Abajas	spring	Jul-2010	451794	4719558	12.0	7.4	3.1	0.5	98	3.0	310	3.5	4.8	0.06	0.03	8.3	0.05	5.30	5.41	-1.10	431	0.774
LA1	Laguillo	spring	Nov-10	447436	4714124	8.5	7.6	12.1	1.5	119	2.1	250	10.8	19.5	0.01	<0.01	123.0	0.08	6.71	6.79	-0.66	538	0.260
EV2	El Vivero	spring	Nov-10	447840	4714727	11.5	7.3	3.0	0.7	90	2.0	277	3.8	4.2	<0.01	<0.01	10.5	0.05	4.81	4.91	-0.95	391	0.270
FH3	Fuente de Hontomin	spring	Nov-10	447725	4736410	17.0	6.7	23.9	3.2	136	2.7	362	15.5	43.6	0.03	<0.01	53.8	0.06	8.17	8.15	0.08	641	2.097
FL4	Fuente Lordujo	spring	Nov-10	448000	4716626	12.5	7.2	2.5	0.5	99	2.2	260	10.6	18.1	0.10	<0.01	22.3	0.09	5.25	5.30	-0.44	415	0.392
FP5	Fuente Peña	spring	Nov-10	446694	4713593	11.5	7.1	2.6	0.8	106	3.1	289	6.8	15.2	0.05	<0.01	15.1	0.09	5.71	5.49	1.93	439	0.103
FCL6	Fuente Castil des Lences	spring	Nov-10	455206	4721182	12.0	7.6	2.8	0.4	72	7.1	244	4.6	3.7	0.02	<0.01	10.0	0.06	4.29	4.37	-0.84	344	n.d.
PDS7	Fuente Poza De La Sal	spring	Nov-10	457740	4723975	10.0	7.5	4.6	0.5	60	6.5	204	7.3	13.0	0.02	<0.01	0.1	0.09	3.77	3.82	-0.67	296	n.d.
RU8	Rio Ubierna	river	Nov-10	443957	4700205	8.5	7.6	13.2	3.9	110	15.5	268	26.9	94.3	0.21	<0.01	19.7	0.10	7.44	7.44	-0.01	552	n.d.
PH9	Fuente Peñahorada	spring	Nov-10	446963	4705202	16.5	7.3	2.6	0.8	80	5.3	246	5.1	6.3	0.03	<0.01	11.7	0.06	4.55	4.50	0.53	358	n.d.
AC11	Manantial Aguas Candidas	spring	Nov-10	458895	4729421	11.0	7.9	2.2	0.6	80	5.7	251	3.8	4.7	0.04	<0.01	12.6	0.06	4.58	4.53	0.64	361	n.d.
FA13	Manantial Fuentona (Abajas 2)	spring	Nov-10	451794	4719558	12.0	7.2	1.6	0.3	89	3.8	287	0.1	0.2	<0.01	<0.01	0.4	0.03	4.84	4.71	1.32	382	0.064
FEA14	Fuente Escobado de Arriba	spring	Nov-10	451576	4733317	9.5	7.8	4.2	1.3	97	1.0	270	5.5	9.7	0.01	<0.01	57.9	0.05	5.17	5.71	-4.98	446	0.003
RH15	Rio Hozabejas	river	Nov-10	456380	4730922	9.0	7.7	2.5	0.9	81	6.4	273	5.0	9.3	0.02	<0.01	1.3	0.04	4.73	4.83	-1.12	380	n.d.
RR16	Rio Oca (Rublacedo de Abajo)	river	Nov-10	458982	4711675	10.0	8.0	3.6	1.3	87	6.5	261	8.8	14.9	0.07	<0.01	17.3	0.06	5.08	5.12	-0.40	400	n.d.
RUT17	Rio Ubierna (Temiño)	river	Nov-10	454567	4701936	8.5	7.7	4.3	5.1	89	3.8	218	18.1	28.0	0.08	<0.01	13.9	0.15	5.11	4.90	2.07	381	n.d.
LA1	Laguillo	spring	Mar-11	447436	4714124	9.0	7.5	14.0	1.1	112	1.4	268	19.0	19.8	<0.01	0.04	61.7	0.08	6.36	6.34	0.16	497	0.739
EV2	El Vivero	spring	Mar-11	447840	4714727	10.0	7.2	3.7	0.8	104	2.0	293	15.0	9.0	0.09	0.01	13.4	0.03	5.55	5.63	-0.74	441	1.894
FH3	Fuente de Hontomin	spring	Mar-11	447725	4736410	8.0	7.2	20.0	4.0	157	3.0	367	27.0	56.7	0.11	0.07	50.8	0.03	9.07	8.78	1.64	686	1.739
FL4	Fuente Lordujo	spring	Mar-11	448000	4716626	7.5	7.3	2.5	0.3	108	2.0	242	11.5	18.7	0.01	0.04	32.8	0.03	5.68	5.21	4.32	418	1.377
FP5	Fuente Peña	spring	Mar-11	446694	4713593	11.0	7.2	2.8	1.5	107	2.2	273	14.0	13.9	0.17	0.04	31.7	0.04	5.70	5.67	0.20	446	1.897
FCL6	Fuente Castil des Lences	spring	Mar-11	455206	4721182	9.0	7.5	2.3	0.4	80	6.2	250	12.0	6.0	<0.01	0.03	0.6	0.01	4.62	4.57	0.53	358	2.137
PDS7	Fuente Poza De La Sal	spring	Mar-11	457740	4723975	8.0	6.9	4.9	0.7	70	7.9	227	14.0	2.1	<0.01	0.03	0.6	0.02	4.38	4.17	2.48	327	0.521
RU8	Rio Ubierna	river	Mar-11	443957	4700205	5.5	7.1	9.7	1.1	109	8.9	273	25.0	51.0	0.01	0.04	1.5	0.03	6.63	6.27	2.82	479	0.491
PH9	Fuente Peñahorada	spring	Mar-11	446963	4705202	11.0	7.3	2.7	0.5	87	5.4	260	6.5	9.4	0.06	0.03	11.2	0.02	4.92	4.82	1.08	383	1.221
RC9	Rio Cantera	river	Mar-11	446149	4703341	10.5	7.3	11.1	1.4	100	5.5	286	22.0	21.0	<0.01	0.05	0.8	0.03	5.98	5.76	1.84	448	0.193
AC11	Manantial Aguas Candidas	spring	Mar-11	458895	4729421	11.5	7.2	2.3	0.7	85	5.6	242	6.1	7.5	<0.01	0.02	6.8	0.01	4.83	4.41	4.59	356	1.159
FA13	Manantial Fuentona (Abajas 2)	spring	Mar-11	451794	4719558	10.5	6.8	1.7	0.3	101	2.9	289	8.0	5.8	<0.01	0.02	9.8	0.06	5.38	5.24	1.26	419	0.813

Table 1
(*Continued*)

Sample	Locality	type	Date	Est	North	Temp.	pH	Na	K	Ca	Mg	HCO_3	Cl	SO_4	F	Br	NO_3	NH_4	Σcat	Σan	Err. %	TDS	Free CO_2
RR16	Rio Oca (Rublacedo de Abajo)	river	Mar-11	458982	4711675	6.5	7.9	4.0	1.0	98	10.3	268	16.0	18.6	0.13	0.04	18.2	0.02	5.95	5.53	3.70	434	2.499
RUT17	Rio Ubierna (Temiño)	river	Mar-11	454567	4701936	5.0	7.9	7.8	0.7	112	3.1	267	24.0	27.0	<0.01	0.04	2.9	0.04	6.22	5.66	4.65	445	0.997
RCM18	Rio Cantera 2	river	Mar-11	446218	4704360	10.0	7.6	12.2	1.8	101	6.9	276	23.0	24.0	<0.01	0.05	0.9	0.03	6.20	5.69	4.27	446	0.560
LA1	Laguillo	spring	Apr-11	447436	4714124	10.0	7.6	11.0	0.9	115	1.2	281	9.4	16.1	0.07	<0.01	44.8	n.d.	6.35	5.92	3.48	479	n.d.
EV2	El Vivero	spring	Apr-11	447840	4714727	n.d.	7.3	3.4	0.8	109	1.9	288	5.7	7.2	0.11	<0.01	12.9	n.d.	5.78	5.24	4.87	429	n.d.
FH3	Fuente de Hontomin	spring	Apr-11	447725	4736410	9.0	7.1	23.6	3.9	167	0.8	389	23.4	63.3	0.12	<0.01	47.7	n.d.	9.54	9.13	2.22	719	n.d.
FP5	Fuente Peña	spring	Apr-11	446694	4713593	11.5	7.2	3.1	0.8	118	2.6	281	9.9	15.8	0.34	<0.01	38.8	n.d.	6.26	5.84	3.55	470	n.d.
EVR	El Vivero Rojo	spring	Apr-11	447840	4714727	11.5	n.d.	6.8	0.5	152	2.9	425	9.6	5.4	0.09	<0.01	2.1	n.d.	8.15	7.38	4.97	602	n.d.

Source: Error is calculated according to Appelo and Postma (1993).
TDS: Total Dissolved Solids; n.d.: not determined. The sum of cations (Σcat) and anions (Σan) are in meq/L, free-CO_2 is in mmol/L. All the other values are in mg/L.

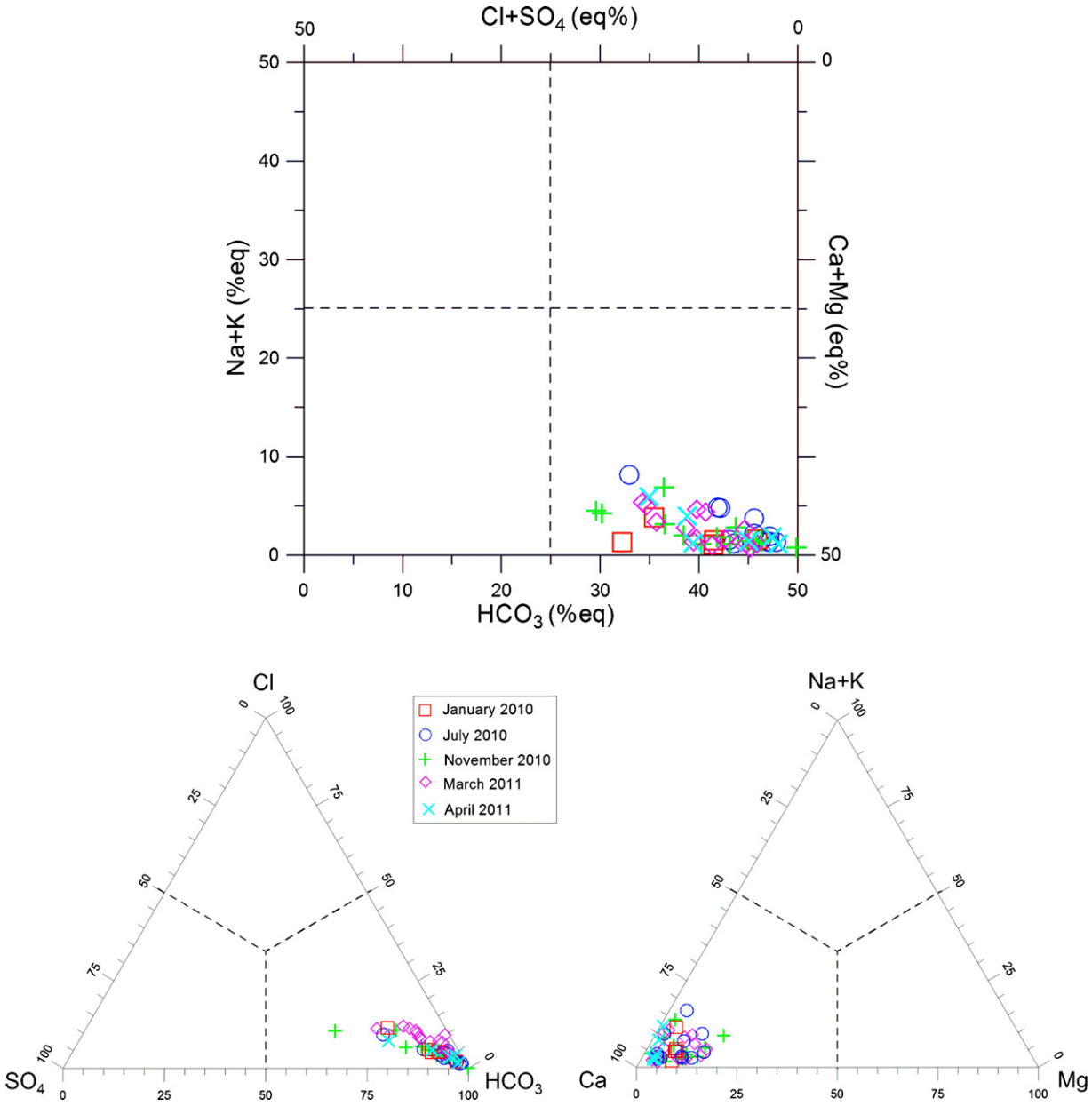

Fig. 2. Square and triangular diagrams for the HH waters, which are grouped according to the period of sampling.
Source: Langelier and Ludwig (1942).

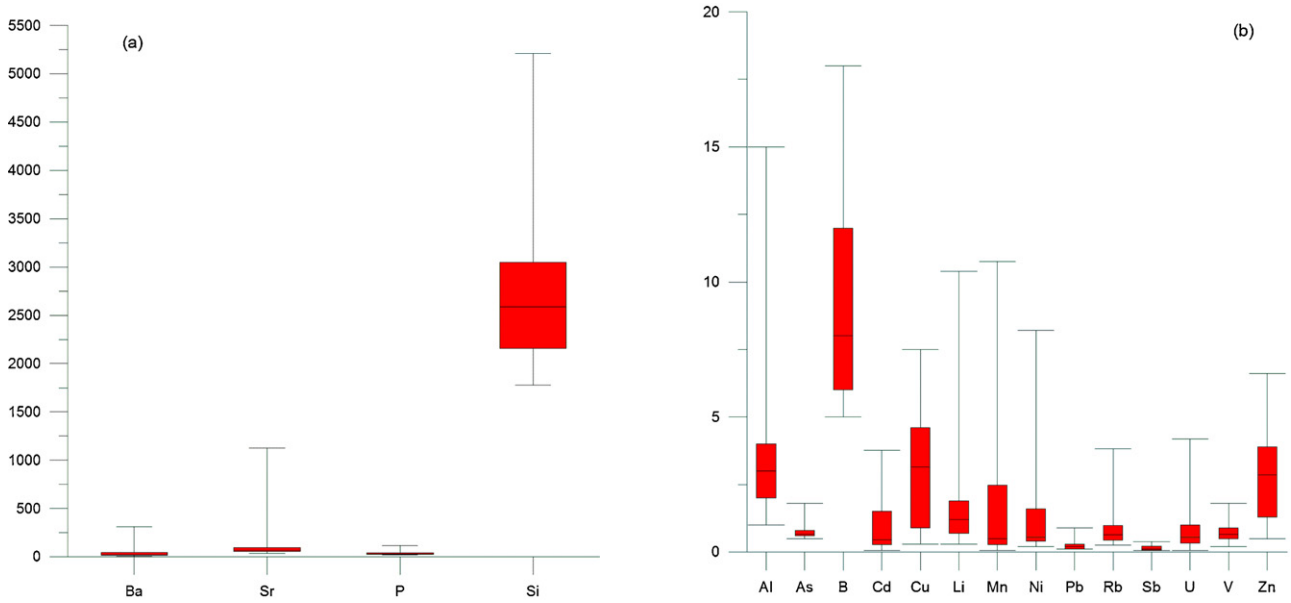

Fig. 3. Box-plot diagrams of trace element concentrations from the HH waters. Values are in μg/L.

method of Coleman et al. (1982). The analytical error for $\delta^{18}O$ and $\delta^{2}H$ was ±0.1 and ±1‰, respectively. The $^{13}C/^{12}C$ ratios of Total Dissolved Inorganic Carbon (TDIC, expressed as δ^{13}C-TDIC‰ V-PDB) were determined with a Finningan Delta Plus XL mass spectrometer on CO_2 produced by the reaction of 3–5 mL of water (depending on the alkalinity) with 2 mL of anhydrous phosphoric acid in pre-evacuated containers (Salata et al., 2000). The recovered CO_2 was analyzed after a two-step extraction and purification procedures by using liquid N_2 and a solid-liquid mixture of liquid N_2 and trichloroethylene (e.g. Evans et al., 1998; Vaselli et al., 2006), respectively. The analytical error for δ^{13}C-TDIC was ±0.1‰.

Chemical gas composition (CO_2, N_2, O_2, Ar, Ne, H_2 and He) in the gas vial headspace was determined with a Shimadzu 15a gas chromatograph equipped with a Thermal Conductivity Detector (TCD), while CH_4 was analyzed with a Shimadzu 14a gas chromatograph with a Flame Ionization Detector (FID). The gas concentrations in the liquid phase were calculated according to the Henry Law (Tassi et al., 2008, 2009; Vaselli et al., 2006). The analytical error was ≤5%.

The $^{13}C/^{12}C$ ratio of dissolved CO_2 (expressed as δ^{13}C-CO_2‰ V-PDB) was determined in the separated gas phase stored in the sampling flask headspace. The carbon isotopic ratio in CO_2 was measured with a Finningan Delta S mass spectrometer after standard extraction and purification procedures by using two cryogenic traps as previously described for δ^{13}C-TDIC (Evans et al., 1998; Vaselli et al., 2006). Analytical error was ±0.05.

To calculate the δ^{13}C values of dissolved CO_2 (δ^{13}C-CO_2) from the measured δ^{13}C ($\delta^{13}C_{meas}$), the carbon isotope fractionation due to liquid-to-gas transfer of CO_2 was quantified by using the ε_1 factor for the gas-water equilibrium (Zhang et al., 1995a), as follows:

$$\varepsilon_1 = \delta^{13}\text{C-CO}_2 - \delta^{13}C_{meas} = (0.0049 \times T) - 1.31 \quad (1)$$

The δ^{13}C-TDIC values were computed by combining the δ^{13}C values of the main inorganic carbon species (HCO_3^- and CO_2). Isotopic fractionation caused by the reaction between dissolved CO_2 and HCO_3^- is quantified by the enrichment factor (ε_2), as follows (Mook et al., 1974):

$$\varepsilon_2 = \delta^{13}\text{C-HCO}_3^- - \delta^{13}\text{C-CO}_2 = 9483/T(K) - 23.9 \quad (2)$$

The theoretical $\delta^{13}C_{TDIC}$ values ($\delta^{13}C_{TDICcalc}$) were computed, as follows:

$$\delta^{13}C_{TDICcalc} = \delta^{13}\text{C-CO}_2 + \varepsilon_2 \times (HCO_3^-)/[(HCO_3^-) + (CO_2)] \quad (3)$$

With the exception of the January 2010 sampling, the $\delta^{13}C_{TDIC}$ values were calculated according to equations (2) and (3). Finally, pCO_2, element speciation, saturation index (SI) and ionic activity were calculated using the aqueous speciation model EQ3/6 (Wolery and Jarek, 2003).

4. Results

4.1. Water chemistry

The chemical composition of the sampled waters (N = 52) is listed in Table 1. Temperatures were between 5 and 19 °C as a function of the sampling period. The pH values and the Total Dissolved Solids (TDS) ranged between 6.7 to 8.2 and 296 to 742 mg/L, respectively. The square (Langelier and Ludwig, 1942) and the HCO_3^--Cl^--SO_4^{2-} and Ca^{2+}-Mg^{2+}-($Na^+ + K^+$) ternary classification diagrams are reported in Fig. 2, where the sampled waters are distinguished according to the period of sampling. The HH water samples are $Ca^{2+}(Mg^{2+})$-HCO_3^- in composition, typical of surface and shallow underground waters (e.g. Drever, 1997). In the anion ternary diagram they show a nearly constant SO_4^{2-}/Cl^- ratio (Fig. 2b), whereas in that of the cations (Fig. 2b) they cluster around the Ca^{2+} vertex with a relatively variable Na/Mg ratio. No significant chemical differences are recorded between surface and spring waters.

Fluoride and Br^- contents were generally <0.7 and 0.08 mg/L, respectively. Ammonium was characterized by concentrations <0.15 mg/L, whereas those of NO_3^- had a large variability, ranging from 0.1 to 123 mg/L. The spring discharges, located close to the HH oil wells, showed the highest NO_3^- values among the whole dataset.

Trace element concentrations are listed in Table 2, while the respective box-plot diagrams are reported in Fig. 3. The highest concentrations were observed for Si (up to 5210 μg/L), Sr (up to 1125 μg/L), Ba (up to 312 μg/L) and P (up to 117 μg/L) (Fig. 3a), whereas all the other elements were <18 μg/L (Fig. 3b) and often

Table 2
Trace element concentrations (in μg/L) for the HH waters.

Sample	Date	Al	As	B	Ba	Cd	Co	Cr	Cs	Cu	Fe	Li	Mn	Ni	P	Pb	Rb	Sb	Se	Si	Sr	Tl	U	V	W	Zn
LA1	Jan-10	3	<0.5	9	16	0.05	0.04	<0.5	0.03	3.5	<10	0.7	10.8	5.8	<20	<0.1	1.1	0.12	<0.5	1839	52	0.01	0.41	0.9	<0.02	6.6
EV2	Jan-10	<1	<0.5	<5	71	2.60	<0.02	1.8	0.01	0.3	<10	0.8	<0.05	<0.2	<20	<0.1	1.2	<0.05	<0.5	2799	52	<0.01	<0.02	0.7	<0.02	1.2
FH3	Jan-10	<1	0.8	13	268	0.32	<0.02	<0.5	<0.01	1.6	<10	2.3	<0.05	<0.2	<20	<0.1	3.4	0.28	1.3	3693	93	0.02	3.21	1.7	<0.02	0.5
FL4	Jan-10	<1	<0.5	6	17	1.88	0.02	<0.5	<0.01	2.2	11	1.3	<0.05	<0.2	<20	<0.1	0.3	0.08	<0.5	2342	65	<0.01	0.54	0.4	<0.02	1.3
FP5	Jan-10	<1	0.6	8	27	1.05	0.04	2.6	<0.01	1.1	<10	1.3	<0.05	5.7	<20	<0.1	0.6	<0.05	<0.5	2892	57	<0.01	0.06	0.5	<0.02	<0.5
LA1	Jul-10	4	<0.5	5	17	0.30	0.06	<0.5	<0.01	4.9	<10	0.9	0.7	1.1	23	<0.1	0.6	0.22	<0.5	4095	69	<0.01	0.75	1.2	<0.02	4.8
EV2	Jul-10	1	<0.5	<5	71	<0.05	<0.02	<0.5	0.04	4.2	<10	0.5	<0.05	<0.2	<20	<0.1	1.2	<0.05	<0.5	2650	54	<0.01	0.35	0.7	<0.02	2.8
FH3	Jul-10	2	0.7	16	313	<0.05	<0.02	<0.5	<0.01	5.1	<10	1.9	<0.05	<0.2	32	0.3	3.6	0.39	0.6	4014	96	0.04	4.19	1.8	<0.02	3.2
FL4	Jul-10	1	<0.5	<5	23	<0.05	<0.02	<0.5	<0.01	4.3	<10	2.6	<0.05	<0.2	<20	0.1	0.4	0.06	<0.5	3071	93	<0.01	0.60	0.3	<0.02	2.9
FP5	Jul-10	3	<0.5	8	33	2.29	0.03	<0.5	<0.01	4.6	<10	1.7	<0.05	<0.2	28	<0.1	0.6	<0.05	<0.5	3676	78	<0.01	0.58	0.5	<0.02	3.2
FCL6	Jul-10	2	0.6	<5	7	0.25	<0.02	<0.5	<0.01	6.1	<10	0.7	0.1	1.0	<20	0.2	0.7	<0.05	<0.5	2103	37	<0.01	0.28	0.7	<0.02	5.4
PDS7	Jul-10	10	0.7	7	11	0.30	0.03	<0.5	<0.01	4.7	<10	1.3	1.8	0.5	32	0.2	0.8	<0.05	<0.5	2875	70	<0.01	0.62	0.6	<0.02	5.3
RU8	Jul-10	3	1.8	14	27	0.51	0.06	<0.5	<0.01	2.5	<10	4.2	2.9	<0.2	24	<0.1	0.7	0.17	<0.5	3930	490	<0.01	1.00	1.2	<0.02	1.9
PH9	Jul-10	3	<0.5	7	6	0.07	<0.02	<0.5	<0.01	4.9	<10	0.5	<0.05	0.9	21	0.2	0.4	<0.05	<0.5	2093	91	<0.01	0.59	1.2	<0.02	3.7
RC9	Jul-10	5	0.7	10	13	0.46	0.02	<0.5	<0.01	3.3	<10	1.7	0.4	<0.2	<20	0.1	0.6	<0.05	<0.5	2979	94	<0.01	0.64	1.1	<0.02	2.7
AC11	Jul-10	2	<0.5	<5	20	0.38	<0.02	<0.5	<0.01	3.5	<10	1.1	<0.05	2.2	<20	<0.1	0.8	<0.05	<0.5	2337	66	<0.01	0.41	0.6	<0.02	3.2
FA12	Jul-10	2	<0.5	5	8	0.60	<0.02	<0.5	<0.01	4.2	<10	0.4	0.4	0.8	<20	<0.1	0.4	<0.05	<0.5	2054	42	<0.01	0.29	0.6	<0.02	3.0
LA1	Nov-10	2	<0.5	<5	19	1.10	<0.02	<0.5	<0.01	3.7	<10	1.0	2.7	0.6	<20	<0.1	1.0	0.17	<0.5	2395	62	0.01	0.50	0.8	<0.02	4.5
EV2	Nov-10	2	<0.5	<5	58	0.39	<0.02	<0.5	0.03	3.8	<10	0.6	0.5	0.3	<20	<0.1	1.0	<0.05	<0.5	2620	41	<0.01	0.26	0.6	<0.02	3.0
FH3	Nov-10	2	0.5	13	193	1.98	<0.02	<0.5	<0.01	4.9	<10	1.3	0.4	1.0	33	<0.1	2.4	0.27	<0.5	3600	66	0.02	2.59	1.4	<0.02	3.9
FL4	Nov-10	1	<0.5	<5	20	0.35	<0.02	<0.5	<0.01	3.0	<10	2.4	0.2	0.3	21	0.1	0.5	<0.05	<0.5	3047	76	<0.01	0.40	0.3	<0.02	2.2
FP5	Nov-10	1	<0.5	5	28	0.17	<0.02	<0.5	<0.01	2.7	<10	1.3	0.3	0.2	23	<0.1	0.5	<0.05	<0.5	3302	65	<0.01	0.41	0.4	<0.02	2.0
FCL6	Nov-10	4	<0.5	<5	6	0.28	<0.02	<0.5	<0.01	6.0	<10	0.3	0.1	0.3	<20	0.2	0.6	<0.05	<0.5	2564	34	<0.01	0.24	0.7	<0.02	5.5
PDS7	Nov-10	1	<0.5	<5	9	0.36	0.03	<0.5	<0.01	4.1	<10	1.0	3.8	0.4	<20	<0.1	0.7	0.06	<0.5	2631	60	<0.01	0.40	0.3	<0.02	3.5
RU8	Nov-10	2	1.5	18	28	2.69	0.02	<0.5	<0.01	4.7	<10	10.4	3.8	<0.2	20	<0.1	1.3	0.23	<0.5	5210	1125	<0.01	1.19	0.7	<0.02	4.1
PH9	Nov-10	2	<0.5	<5	6	0.19	<0.02	<0.5	<0.01	4.8	<10	0.4	0.1	0.5	21	<0.1	0.4	<0.05	<0.5	2297	72	<0.01	0.48	0.9	<0.02	3.6
AC11	Nov-10	2	<0.5	<5	15	0.19	<0.02	<0.5	<0.01	3.6	12	0.5	0.4	0.4	<20	<0.1	0.6	<0.05	<0.5	2494	48	<0.01	0.30	0.4	<0.02	2.9
FA13	Nov-10	2	<0.5	<5	7	0.25	<0.02	<0.5	<0.01	3.5	<10	0.4	<0.05	<0.2	<20	<0.1	0.4	<0.05	<0.5	2084	35	<0.01	0.24	0.5	<0.02	2.7
FEA14	Nov-10	7	<0.5	<5	27	1.30	<0.02	<0.5	<0.01	7.5	<10	1.2	0.2	0.4	27	0.3	1.8	0.08	<0.5	2302	62	<0.01	0.21	0.6	<0.02	5.9
RH15	Nov-10	2	<0.5	<5	16	0.70	<0.02	<0.5	<0.01	4.6	<10	0.7	0.5	0.4	27	<0.1	1.0	<0.05	<0.5	2645	54	<0.01	0.33	0.3	<0.02	4.0
RR16	Nov-10	2	<0.5	5	43	0.21	<0.02	<0.5	<0.01	4.5	<10	1.9	0.4	0.3	20	<0.1	0.6	0.07	<0.5	3334	104	<0.01	1.05	0.7	<0.02	3.0
RUT17	Nov-10	15	<0.5	9	46	0.40	0.03	<0.5	<0.01	5.0	<10	3.5	1.2	0.5	31	<0.1	3.8	0.1	<0.5	3332	173	<0.01	2.51	0.5	<0.02	4.0
LA1	Mar-11	5	<0.5	<5	16	1.18	0.03	<0.5	<0.01	1.0	<10	0.8	1.8	<0.2	33	0.1	0.9	0.14	<0.5	1791	56	<0.01	0.64	0.9	<0.02	2.2
EV2	Mar-11	2	0.6	5	65	1.51	<0.02	<0.5	0.03	0.5	<10	0.7	10.0	0.6	27	<0.1	1.0	0.11	<0.5	2200	51	<0.01	0.92	1.1	<0.02	<0.5
FH3	Mar-11	9	0.6	14	263	1.42	<0.02	0.8	<0.01	1.7	<10	1.8	0.5	7.8	36	0.1	2.6	0.28	0.8	3019	80	0.03	3.43	1.4	<0.02	1.7
FL4	Mar-11	11	<0.5	<5	16	0.68	<0.02	<0.5	<0.01	0.7	<10	1.2	0.2	<0.2	23	<0.1	0.3	0.06	<0.5	1950	68	<0.01	0.51	0.2	<0.02	0.7
FP5	Mar-11	3	<0.5	5	29	3.30	<0.02	<0.5	<0.01	0.9	<10	1.3	0.2	8.2	30	<0.1	0.6	<0.05	<0.5	2246	56	<0.01	0.42	0.4	<0.02	1.3
FCL6	Mar-11	13	<0.5	<5	8	0.33	<0.02	<0.5	<0.01	1.8	16	0.4	0.7	3.0	39	0.3	0.6	<0.05	<0.5	2039	37	<0.01	0.30	0.8	<0.02	2.7
PDS7	Mar-11	2	0.7	8	12	1.88	<0.02	<0.5	<0.01	0.6	<10	1.1	5.2	0.5	39	<0.1	1.0	<0.05	<0.5	2569	63	<0.01	0.63	0.5	0.06	0.6
RU8	Mar-11	4	1.1	9	26	1.68	<0.02	<0.5	<0.01	1.1	<10	4.8	0.9	<0.2	50	<0.1	0.4	0.15	<0.5	2324	580	<0.01	1.24	0.6	<0.02	1.0
PH9	Mar-11	5	<0.5	<5	6	2.29	<0.02	<0.5	<0.01	0.7	<10	0.6	0.3	<0.2	38	0.2	0.4	<0.05	<0.5	1903	81	0.01	0.56	1.0	<0.02	3.9
RC9	Mar-11	3	0.5	9	18	n.d.	<0.02	<0.5	<0.01	0.8	<10	2.0	2.5	<0.2	40	<0.1	0.6	0.05	<0.5	2113	111	0.02	0.90	0.7	<0.02	<0.5
AC11	Mar-11	3	<0.5	<5	19	3.77	<0.02	<0.5	<0.01	0.8	<10	0.5	0.7	0.2	40	0.1	0.6	<0.05	<0.5	2512	54	<0.01	0.35	0.5	<0.02	0.7
FA13	Mar-11	2	<0.5	<5	7	0.65	<0.02	<0.5	<0.01	0.5	<10	0.3	0.1	<0.2	35	<0.1	0.4	<0.05	<0.5	1961	36	<0.01	0.30	0.6	<0.02	<0.5
RR16	Mar-11	5	0.6	7	78	0.41	<0.02	<0.5	<0.01	0.8	<10	3.3	0.6	1.4	34	0.1	0.3	0.09	0.5	2742	173	<0.01	1.96	1.2	<0.02	1.5
RUT17	Mar-11	3	<0.5	6	31	0.56	<0.02	<0.5	<0.01	0.9	<10	1.4	0.5	<0.2	30	0.3	0.3	0.09	<0.5	1775	124	<0.01	1.66	0.6	<0.02	0.8
RCM18	Mar-11	4	0.6	11	19	n.d.	0.03	<0.5	<0.01	1.0	<10	2.4	7.1	0.4	49	<0.1	0.7	0.06	<0.5	2158	135	0.01	1.06	0.9	<0.02	1.2
LA1	Apr-11	3	<0.5	<5	15	0.16	0.02	<0.5	<0.01	1.2	<10	0.9	2.6	1.6	49	0.9	0.6	0.11	<0.5	2267	58	<0.01	0.63	<0.2	<0.02	2.2
EV2	Apr-11	4	<0.5	<5	76	0.12	<0.02	<0.5	0.04	0.9	<10	0.7	2.3	<0.2	34	<0.1	1.2	0.06	0.6	2808	60	<0.01	0.30	<0.2	0.07	5.4
FH3	Apr-11	2	<0.5	12	271	<0.05	<0.02	<0.5	<0.01	6.1	<10	1.7	0.3	2.0	117	0.4	2.5	0.28	0.8	3732	86	0.03	3.65	0.4	<0.02	1.5
FL4	Apr-11	<1	<0.5	<5	20	<0.05	<0.02	<0.5	<0.01	0.9	<10	2.0	0.2	0.5	21	<0.1	0.3	<0.05	<0.5	2609	84	<0.01	0.32	<0.2	<0.02	0.6
FP5	Apr-11	1	<0.5	<5	30	0.06	<0.02	<0.5	<0.01	2.9	<10	1.3	0.2	<0.2	55	0.2	0.5	<0.05	<0.5	2795	64	<0.01	0.48	<0.2	<0.02	0.7

Table 3
Chemical composition of the dissolved gases in the HH waters; gas concentrations are in % by volume, while the sum of the dissolved gases (ΣDG) is in mmol/L.

Sample	Date	CO_2	N_2	O_2	Ar	CH_4	Ne	He	H_2	ΣDG
LA1	Jan-10	44.8	53.6	0.4	1.3	0.0131	0.00055	0.00193	<0.00001	1.20
EV2	Jan-10	21.7	59.3	17.5	1.5	0.0162	0.00065	<0.00001	<0.00001	1.27
FH3	Jan-10	63.0	34.7	1.4	0.8	0.0110	0.00043	0.00243	<0.00001	1.64
FL4	Jan-10	4.4	71.8	22.0	1.7	0.0000	0.00076	<0.00001	<0.00001	0.87
FP5	Jan-10	3.4	68.2	26.7	1.6	0.0152	0.00076	<0.00001	<0.00001	1.31
EV2	Jul-10	18.9	69.4	9.9	1.8	<0.0001	0.00107	<0.00001	<0.00001	1.87
FH3	Jul-10	50.6	43.1	5.2	1.0	0.0233	0.00039	<0.00001	<0.00001	2.58
FL4	Jul-10	5.2	72.8	20.4	1.6	<0.0001	<0.00001	<0.00001	<0.00001	0.81
FP5	Jul-10	16.7	71.0	11.9	1.8	<0.0001	<0.00001	<0.00001	<0.00001	0.93
FCL6	Jul-10	20.0	67.5	10.7	1.7	<0.0001	0.00069	<0.00001	<0.00001	1.46
PDS7	Jul-10	13.9	71.7	12.8	1.7	<0.0001	0.00060	<0.00001	<0.00001	1.67
PH9	Jul-10	19.2	67.1	12.0	1.7	<0.0001	<0.00001	<0.00001	<0.00001	0.88
AC11	Jul-10	37.2	60.0	1.3	1.5	0.0229	0.00092	0.00046	0.00046	2.18
FA12	Jul-10	17.8	69.9	10.4	1.9	<0.0001	0.00083	<0.00001	<0.00001	1.21
EV2	Nov-10	15.1	69.2	13.9	1.8	<0.0001	0.00070	<0.00001	<0.00001	1.43
FH3	Nov-10	47.7	46.1	5.0	1.1	0.0297	0.00042	<0.00001	<0.00001	2.36
FL4	Nov-10	2.9	76.4	18.8	1.9	<0.0001	0.00071	<0.00001	<0.00001	0.93
FP5	Nov-10	2.3	71.6	24.4	1.8	0.0073	0.00073	<0.00001	<0.00001	1.37
FCL6	Nov-10	13.4	70.8	14.0	1.8	<0.0001	0.00086	<0.00001	<0.00001	1.16
PDS7	Nov-10	4.2	82.0	11.9	1.9	<0.0001	0.00086	<0.00001	<0.00001	1.17
PH9	Nov-10	15.3	69.0	14.0	1.7	<0.0001	<0.00001	<0.00001	<0.00001	0.92
FA13	Nov-10	7.3	79.6	11.2	2.0	<0.0001	0.00094	<0.00001	<0.00001	1.06
EV2	Mar-11	5.8	69.8	22.6	1.7	0.0084	0.00840	<0.00001	<0.00001	1.19
FH3	Mar-11	24.7	61.0	15.4	1.6	<0.0001	0.00120	<0.00001	<0.00001	1.66
FP5	Mar-11	4.5	67.3	26.6	1.6	0.0078	0.00078	<0.00001	<0.00001	1.28
FL4	Mar-11	4.3	74.7	19.1	1.8	<0.0001	<0.00001	<0.00001	<0.00001	0.82

characterized by contents below the instrumental detection limit. It is worth to mention that the highest concentrations of As were recorded in the Rio Ubierna (RU8) and the Fuente Hontomín (FH3): up to 1.5 and 0.8 μg/L, respectively. Among the heavy metals (Cd, Co, Cr, Cu, Fe, Mn, Ni, Pb, Sb, Se, Tl and Zn), Fe was usually below the detection limit (<10 μg/L), similarly to Co (<0.02 μg/L), Cr (<0.05 μg/L), Pb (<0.1 μg/L), Se (<0.5 μg/L) and Tl (<0.01 μg/L). Cadmium, Cu, Mn and Zn had contents up to few μg/L, while Ni showed concentrations that were mostly <1 μg/L. Large ion lithofile elements, such as Ba, Cs, Rb and Sr, ranged between 6 (FCL 6 and PH9) and 313 (FH3), <0.01 and 0.04 (EV2), 0.3 (FL4, RR16 and RUT17) and 3.8 (RUT17) and 34 (FCL) and 1125 (RU8) μg/L, respectively. The highest Al content was 15 (RUT17) μg/L, although most concentrations clustered around 1 and 5 μg/L, B was ranging between <5 and 16 (FH3) μg/L, Li varied between 0.3 (FCL6 and FA13) and 10.4 (RU8) μg/L, the highest content of U (4.19 μg/L) was recorded at the spring water FH3. Vanadium was always <1.8 (FH3) μg/L.

Table 4
Oxygen (as $\delta^{18}O$‰ V-SMOW), hydrogen (as $\delta^{2}H$‰ V-SMOW), measured TDIC (Total Dissolved Inorganic Carbon, in mol/L) and carbon isotopic composition in the waters and dissolved gases from HH.

ID	Date	$\delta^{18}O$	$\delta^{2}H$	TDIC	$\delta^{13}C$-TDIC	$\delta^{13}C$-CO_2
LA1	Jan-10	−8.0	−49.2	0.0043	−10.1	−19.6
EV2	Jan-10	−8.1	−61.2	0.0047	−10.8	−19.0
FH3	Jan-10	−7.9	−48.5	0.0054	−12.4	−21.3
FL4	Jan-10	−8.9	−60.5	0.0041	−9.2	−20.3
FP5	Jan-10	−9.6	−62.4	0.0044	−11.5	−20.0
EV2	Jul-10	n.d.	n.d.	0.0057	*−11.9*	−19.4
FH3	Jul-10	n.d.	n.d.	0.0066	*−12.8*	−21.6
FL4	Jul-10	n.d.	n.d.	0.0050	*−11.6*	−20.1
FP5	Jul-10	n.d.	n.d.	0.0058	*−12.4*	−19.8
FCL6	Jul-10	n.d.	n.d.	0.0043	*−10.3*	−19.3
PH9	Jul-10	n.d.	n.d.	0.0044	*−8.6*	−18.0
AC11	Jul-10	n.d.	n.d.	0.0045	*−8.5*	−18.0
FA12	Jul-10	n.d.	n.d.	0.0059	*−9.6*	−17.7
LA1	Nov-10	−8.7	−58.6	0.0044	*n.d.*	n.d.
EV2	Nov-10	n.d.	n.d.	0.0048	*−9.7*	−18.6
FH3	Nov-10	−8.8	−58.2	0.0080	*−16.9*	−23.4
FL4	Nov-10	n.d.	n.d.	0.0047	*−10.8*	−19.3
FP5	Nov-10	n.d.	n.d.	0.0048	*−13.3*	−22.5
PDS7	Nov-10	n.d.	n.d.	0.0033	*−9.4*	−19.0
PH9	Nov-10	n.d.	n.d.	0.0040	*−9.7*	−18.5
FA13	Nov-10	n.d.	n.d.	0.0048	*−9.2*	−18.5
EV2	Mar-11	n.d.	n.d.	0.0067	*−13.4*	−20.3
FH3	Mar-11	n.d.	n.d.	0.0078	*−14.5*	−22.1
FL4	Mar-11	n.d.	n.d.	0.0053	*−14.0*	−21.3
FP5	Mar-11	n.d.	n.d.	0.0064	*−14.0*	−20.7

Source: Table 1 by applying equations (2) and (3).
Carbon isotopes in TDIC (Total Dissolved Inorganic Carbon; expressed as $\delta^{13}C$-TDIC‰ V-PDB) for the January 2010 sampling were measured, while those of the other samplings (in italics) are calculated by using the $\delta^{13}C$-CO_2 in the dissolved gas and HCO_3 and free-CO_2 concentrations.

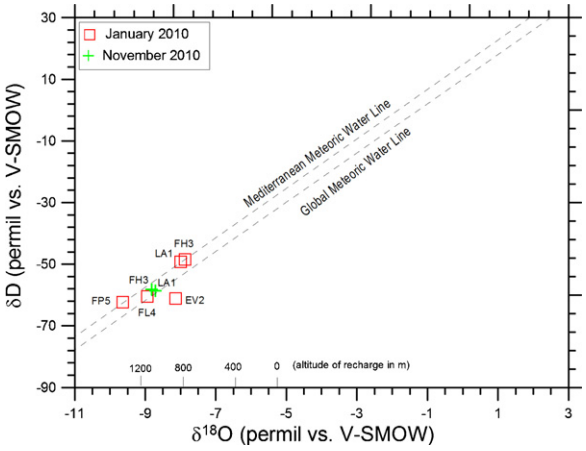

Fig. 4. Hydrogen (as δ^2H‰ V-SMOW) and Oxygen (as δ^{18}O‰ V-SMOW) binary diagram for the HH waters collected in January 2010 and altitude of the meteoric waters recharging the HH shallow hydrological circuits.

4.2. Dissolved gas chemistry

Dissolved gas composition was determined in the springs with the exception of the April 2011 sampling when no measurements were carried out. The chemical composition (in % by volume) and the sum of the dissolved gas concentrations (ΣDG in mmol/L) for the HH waters are listed in Table 3. The total dissolved gas concentration did not exceed 2.6 mmol/L. Most gases were dominated by an atmospheric component since N_2, O_2 and Ar were often the prevailing gases. Nevertheless, carbon dioxide was always >2.3% by vol. and a few samples were characterized by CO_2 concentrations up to 63% by vol. Methane, Ne and He were up to 0.03, 0.008 and 0.002% by vol., respectively, while H_2 was mostly below the instrumental detection limit (<0.00001% by vol.).

4.3. Stable isotopes

The oxygen and hydrogen isotopic ratios in the water molecule (expressed with the δ notation ‰ and referred to V-SMOW) were measured in seven water spring discharges. The δ^{18}O and δ^2H values ranged from −9.6 to −7.9‰ (V-SMOW) and from –62.4 to –48.4‰ (V-SMOW), respectively (Table 4), The δ^{18}O and δ^2H values indicate that the HH waters are of meteoric origin, plotting between the Global (Craig, 1961) and the Mediterranean (Gat and Carmi, 1971) meteoric water lines (Fig. 4). The slightly more positive δ^{18}O value for the EV2 sample was likely due to some evaporative process. The δ^{13}C-CO_2 (expressed with the δ notation ‰ and referred to V-PDB) values in the dissolved gases were rather negative, varying between −23.4 and −17.7‰ (V-PDB). Similar negative values were obtained when considering the measured and calculated δ^{13}C-TDIC values since they were as low as −16.9‰ V-PDB (Table 4).

5. Discussion

5.1. Origin of the dissolved species

The Palaeozoic to Quaternary sedimentary rocks at HH are mainly made up by silicate and carbonate minerals at different proportions. The latter are likely responsible for the chemical composition of the analyzed waters, which show a Ca(Mg)-HCO_3 facies. This is supported by the fact that the HCO_3/(Ca + Mg) (in meq/L) is approaching the stoichiometric value of 1, suggesting that the congruent dissolution of Ca-Mg-bearing carbonate mostly contribute to the chemistry of the HH waters. The relatively low TDS (<800 mg/L) values indicate shallow circulation circuits fed by meteoric water. In order to calculate the hypothetical recharge area at which the meteoric waters are infiltrating, we may assume a vertical gradient of –0.36‰ δ^{18}O/100 m and a value of about −6‰ (V-SMOW) for spring discharging at sea level in the central Mediterranean Sea (Minissale and Vaselli, 2011). This may suggest that the recharge elevation of the springs surrounding the HH area can nearly be set between 800 and 1000 m (Fig. 4).

The chemical composition of surface and shallow waters does not necessarily reflect unambiguously natural geochemical processes. For example, TDS variations in surface waters are the results of combined effects, e.g. lithology and pollution (e.g. Gaillardet et al., 1999; Roy et al., 1999; Han and Liu, 2004). Generally speaking, the concentrations of most major ions are significantly increased due to anthropogenic contamination (e.g. Na^+ = 28%, SO_4^{2-} = 54%, Cl^- = 30%, Ca^{2+} = 9%, K^+ = 7%), e.g. Berner and Berner (1996) and reference therein. It is well established that Na^+ and K^+, Cl^- and NO_3^- and, to a minor extent, Br^- and F^- may be derived from agricultural fertilizers, animal waste, and municipal and industrial sewage; thus, a relationship between increasing TDS and these dissolved species may help to understand the anthropogenic effect on the water chemistry of the HH samples. In this respect, dissolved nitrate in surface and shallow ground waters represents an important geochemical tracer of pollution. Interestingly, the HH waters are characterized by a large variability of NO_3^- concentrations as they span from 0.14 to 123 mg/L, whereas Cl^-, Na^+, SO_4^{2-} and K^+ contents are from 0.10 to 30, 1.6 to 34, 0.22 to 94 and 0.3 to 5.1 mg/L, respectively. Chloride and SO_4^{2-} show a positive correlation between them and with TDS, the highest contents pertaining to Fuente Hontomín (FH3) and Rio Ubierna (RU8) (Table 1). The Cl^-/SO_4^{2-} (mostly <2.8) ratios are generally much lower than in the marine aerosols ($Cl^-/SO_4^{2-}{}_{SW}$ = 6.9 as mg/L). Thus, we may suppose that SO_4^{2-} may have a weak contribution by the interaction with evaporitic minerals (e.g. gypsum) present within the sedimentary rocks that constitute the outcropping rocks in the HH area. Nevertheless, oxidation of sulphide (e.g. FeS_2) minerals cannot be excluded.

According to Widory et al. (2005), nitrate in natural waters commonly occurs at moderate concentrations, i.e. around 10 mg/L, while higher contents are usually indicative of anthropogenic sources. Like Ca and Mg, bicarbonate in rivers and groundwater bodies is derived from natural sources, while pollution contribution is as low as 2% (e.g. Meybeck, 1979). Despite the fact that the HH waters can be regarded as mainly sourced by natural processes, the origin of nitrate deserves a particular attention, this solute showing contents that are commonly related to polluted areas. Therefore, in Fig. 5 TDS (in mg/L) is plotted against the $HCO_3^-/(HCO_3^- + NO_3^-)$ (in mg/L) ratio, the latter parameter considering NO_3^- as mainly related to anthropogenic sources, while HCO_3^- is representative of weathering processes. The variation of the $HCO_3^-/(HCO_3^- + NO_3^-)$ ratio is between 0 and 1. Most water samples have a $HCO_3^-/(HCO_3^- + NO_3^-)$ ratio clustering around 1, indicating that natural processes are the dominating factors for these waters and tend to divert for a concentration of TDS close to 300 mg/L. From this pristine value two trends are recognized (Fig. 5): (1) typical surface/shallow water composition with a TDS value from 300 to nearly 600 mg/L and a $HCO_3^-/(HCO_3^- + NO_3^-)$ ratio ≈1, i.e. dominated by natural sources; (2) relatively contaminated waters, shifted toward low $HCO_3^-/(HCO_3^- + NO_3^-)$ ratios with values down to 0.67 (LA1), and characterized by a NO_3^--rich component, likely related to an anthropogenic source. The Fuente Hontomín (FH3) waters have the highest TDS values and the $HCO_3^-/(HCO_3^- + NO_3^-)$ ratios are between the trend lines (1) and (2), i.e. 0.83 ÷ 0.89. This may be suggesting that NO_3 is derived from an anthropogenic source possibly affected by a Cl-SO_4-rich (deep?) component, this spring being characterized by the highest Cl^- and SO_4^{2-} concentrations among all the investigated samples.

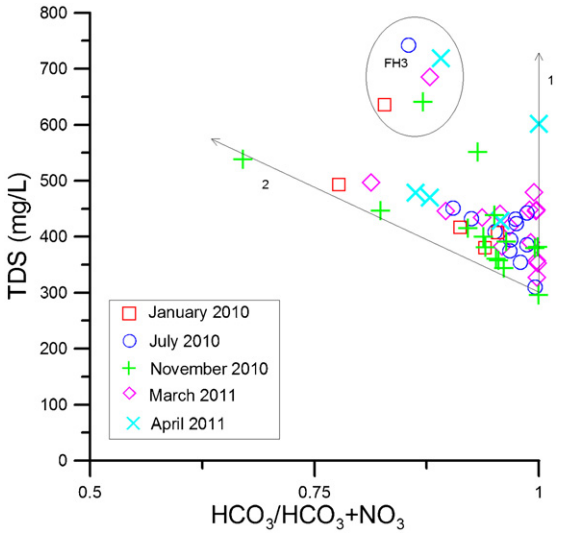

Fig. 5. Total Dissolved Solids (TDS in mg/L) versus $HCO_3^-/(HCO_3^- + NO_3^-)$ ratio for the HH waters. Line 1 represents the contribution of NO_3 to the typical $Ca^{2+}(Mg^{2+})$-HCO_3^- composition of the HH waters; Line 2 refers to an increase of TDS due to slightly longer circulation.

It is worth of noting that similar or even higher Cl^- and SO_4^{2-} contents are also found in the Rio Ubierna (RU8; Table 1). This finding may be explained by the presence of relatively Cl-SO_4-rich water discharges that affect the Rio Ubierna where the NO_3^- concentrations are always below 20 mg/L, indicating for this river a low contribution by anthropogenic sources.

The most probable source of nitrates is likely associated with the attempt to obtain productive systems and integrated to the landscape by the administration of the Castilla-León Region, using N-rich effluents (Macías et al., 2005) to increase the vegetative cover. These effluents were derived by manufacturing processes of explosive materials, such as nitroglycerin, TNT, dynamite, penthrite, by a local factory. After mixing and neutralizing these compounds two wastewaters were obtained both characterized by high concentrations of nitrates (~57,000 mg/L) and extreme pH values (0.5 and 9.0, respectively). A dilution between the two wastewaters was provided to increase the pH values up to 5–6 (Calvo, 2002; Macías et al., 2005) and spread in the territory close to HH. The chemical composition of the effluents was characterized by 1000–3000 mg/L of SO_4^{2-}, 3000–22,000 mg/L of Na^+, whilst the concentrations of Cl^-, Ca^{2+}, Mg^{2+}, K^+ and NH_4^+ were from 0.1 to 500 mg/L (Macías et al., 2005). It is interesting to mention that the metal contents in the effluents are relatively low, ranging from <0.1 (Mn, As and Zn) to 13 (Al) mg/L. Apparently, this practice was abandoned in 2007.

As previously mentioned, trace elements concentrations in the studied waters did not show any peculiar or anomalous value (Table 2), being most of them being characterized by contents that approached the instrumental detection limit or were below it and thus, likely related to the geological environment through which they move, as observed worldwide (e.g. Kreamer et al., 1996 and references therein). However, when compared to the studied waters, Fuente Hontomín (FH3) and Rio Ubierna (RU8) showed relatively higher concentrations of As and B (up to 0.8 and 1.8 and up to 16 and 18 μg/L, respectively, Table 2) and U (up to 4.19 μg/L) at FL4 that may possibly be related to a deeper source, as previously stressed for Cl^- and SO_4^{2-}. High Ba concentrations in FH3 were found to be between 193 and 313 μg/L, whereas those in RU8 were similar to the other water samples, likely due to the fact that this element is easily removed in surface waters, as it tends to precipitate.

It can be speculated that some main and trace elements might be related to the effects of the NO_3-rich effluents. However, if we consider that the highest concentration of NO_3^-, recorded in FH3, was 123 mg/L, this would suggest a dilution of about 1/460 with respect to the content of NO_3^- in the effluents (ca. 57,000 mg/L). If this dilution coefficient is applied to those elements, such as As, that were considered to be related to a deep source, an anthropogenic contribution of <0.2 μg/L is expected, and thus, negligible with respect to the concentrations found in FH3 and RU8. Even for the major solutes (e.g. Cl^-, Ca^{2+} and Mg^{2+}) the contribution by this anthropogenic source is to be considered negligible when compared with the concentrations found in the sampling sites close to the HH area. Only SO_4^{2-} and Na^+ concentrations can be related to the NO_3-rich effluents; however the relatively constant SO_4^{2-}/Cl^- ratio (Fig. 2b) observed for the investigated water samples does not support this hypothesis.

The water samples discharging close to the Hontomín oil wells and monitored during the five campaigns carried out in this area, i.e. Fuente Laguillo (LA1), El Vivero (EV2), Fuente Hontomín (FH3), Fuente Lordujo (FL4) and Fuente Peña (FP5), did not show seasonal variations in terms of geochemical facies, although some solutes had significant variations with time. Furthermore, selected molar ratios indicate different sources of the solutes, due to either differences in the lithological features interacting with the water discharges or anthropogenic inputs. Molar ratios are particularly well suited to distinguish waters interacting with different sedimentary rocks; moreover, these ratios are independent from flow rates, dilution and evaporative effects (e.g. Négrel et al., 1993; Zhang et al., 1995b; Gaillardet et al., 1997; Han and Liu, 2004). As an example, in Fig. 6 NO_3^- concentrations (in mg/L) and HCO_3^-/NO_3^- and Ca^{2+}/Na^+ molar ratios versus sampling date are reported. With the exception of the EV2 water samples that maintain a relatively constant and low NO_3^- content with time, all the other samples have higher concentrations (Table 1) of nitrate and a larger variability with time. While FL4 and FP5 show a slight tendency to increase their NO_3^- contents, FH3 shows a marked decrease. On the other hand, LA1 is abruptly oscillating from 30 to 123 mg/L without a clear seasonal correlation (Fig. 6a). These different trends appear more evident when the HCO_3^-/NO_3^- molar ratios are taken into account since this ratio is achieving the highest values for EV2, followed by those of FL4 and FP5, whereas they are <10 for LA1 and FH3 (Fig. 6b). This implies that these two water discharges are the most prone to NO_3^- pollution. It is remarkable that LA1 and FH3 show the lowest Ca/Na molar ratios (Fig. 6c), likely due to both different lithological (silicate minerals) and anthropogenic contributions, as supported by their low HCO_3^-/Cl^- and HCO_3^-/SO_4^{2-} values with time (not shown).

5.2. Origin of the dissolved gases

The relatively shallow circuits that characterize the HH waters are also evident when considering the dissolved species since they are dominated by N_2, O_2 and Ar. Furthermore the N_2/Ar ratios are clustering around 38 as shown in Fig. 7a, this value corresponding to that of ASW (Air Saturated Water) at 20 °C (e.g. Giggenbach, 1995). The N_2/O_2 ratios are usually higher than that in ASW (1.88) due to O_2 consumption underground as oxidative processes are occurring, this is particularly true for those samples that have values >20 (Table 3). However, the presence of a non-atmospheric source for the dissolved gases is evidenced in the N_2 versus CO_2 (in % by vol.) binary diagram (Fig. 7b), where an inverse significant correlation ($R^2 = 0.87$) is observed. The presence of CH_4, although at relatively low concentrations (Table 3), further corroborates this observation. According to the $\delta^{13}C$-CO_2 values, which are characterized by negative value (<−17.7‰ V-PDB), a biogenic source likely related to the soil zone, whose values can be as low as <−25‰

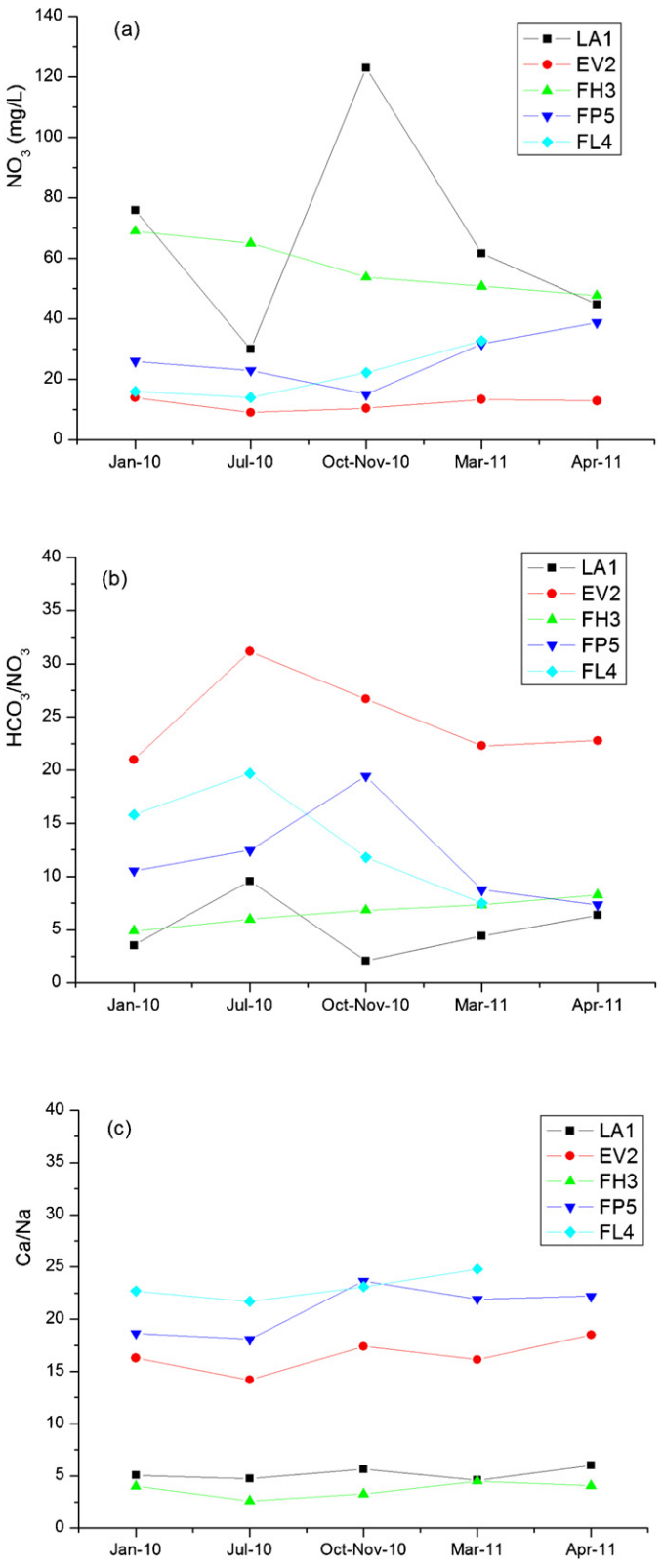

Fig. 6. Temporal variations of (a) NO_3^- concentrations (in mg/L) and (b) HCO_3^-/NO_3^- and (c) Ca^{2+}/Na^+ molar ratios for the monitored water samples (LA1, EV2, FH3, FL4 and FP5) during the period of January 2010 and April 2011.

V-PDB (e.g. Rollinson, 1993 and references therein), can be invoked (see below), although no carbon and hydrogen isotopic data are presently available for CH_4.

5.3. Processes governing water composition

SI, activity values, $\log(pCO_2)$ and measured and calculated TDIC (in mol/L) are reported in Table 5. The SI confirms that the major process controlling the surface and shallow water composition is the dissolution of calcite and dolomite (SI_{cal} is from −0.63 to +1.06 and SI_{dol} from −1.1 to +2.26), whereas SI for the main silicatic minerals is largely negative. Thus, meteoric waters as interact with the substratum become saturated in calcite and to a lesser extent dolomite; consequently, a Ca(Mg)-HCO_3 composition is attained in the initial stages of water–rock interaction processes due to calcite dissolution even in small amount. This is related to the fact that the dissolution rate of calcite is 2–6 orders of magnitude higher than that of Al-silicates, depending upon the pH (Stumm and Morgan, 1996 and references therein).

Activity plots represent a very effective tool for investigating the saturation state of a number of waters with respect to several, relevant solid phases, provided that temperature and pressure are kept constant or nearly so (Helgeson, 1968; Bowers et al., 1984). The use of activity plots also allows a quick evaluation of the effects of mixing in the solid state, as the stability field limits of solid mixture end-members are taken into account. The activity plots for the Na_2O–Al_2O_3–SiO_2–H_2O (Fig. 8a), K_2O–Al_2O_3–SiO_2–H_2O (Fig. 8b), MgO–Al_2O_3–SiO_2–H_2O (Fig. 8c), and CaO–Al_2O_3–SiO_2–H_2O (Fig. 8d) systems were plotted assuming conservation of Al in the solid phases; as a consequence, among clay minerals only kaolinite and beidellites were considered, with the exception Mg-saponite whose stability field is shown in the activity plot for the MgO–Al_2O_3–SiO_2–H_2O system (Fig. 8c). The theoretical grids were computed for 15 °C and 1.013 bar. Activities of the different ions and SiO_2(aq) were computed for each water sample by means of EQ3/6 code (Wolery and Jarek, 2003) (Table 5).

The HH waters are found in the stability field of kaolinite and most waters are saturated with dolomite and calcite (Fig. 8c and d). The activity plots for the MgO-SiO_2-Al_2O_3-H_2O and CaO-SiO_2-Al_2O_3-H_2O chemical systems (Fig. 8c and d) also report the saturation lines for calcite and dolomite corresponding to $\log f_{CO_2}$ values of −1 and −3, confirming the control of calcite (or Ca-carbonates) and dolomite on Ca^{2+} and Mg^{2+} activity, respectively. Basically, calcite and dolomite saturation acts as a sort of geochemical barrier in determining the possible attainment of saturation with primary Ca-silicates, e.g. anorthite, at very low CO_2 fugacity. These waters are indeed strongly undersaturated with respect to the most important Na-, Mg- and Ca-bearing primary minerals, i.e., albite, and anorthite, and diopside, although some samples approach saturation for Mg-Saponite, muscovite and K-feldspar (Fig. 8a–c).

5.4. Total dissolved inorganic carbon (TDIC) and pCO_2

Calcite and dolomite dissolution affecting the studied waters are strictly controlled by pCO_2. The range of variation of the pCO_2 values is directly related, through the mass action law, to the content of dissolved carbonic acid, H_2CO_3, which is the main acidic substance driving mineral dissolution reactions in most natural environments, as follows:

$$H_2CO_3^* = CO_2(g) + H_2O \quad K_H \frac{f_{CO_2}}{a_{H_2CO_3}} = \left(\frac{F_{CO_2}}{m_{H_2CO_3^*} \gamma_{H_2CO_3^*}} \right) = 10^{+1.47} \quad 25\,^\circ C \tag{4}$$

where K_H is the Henry constant of gaseous CO_2.

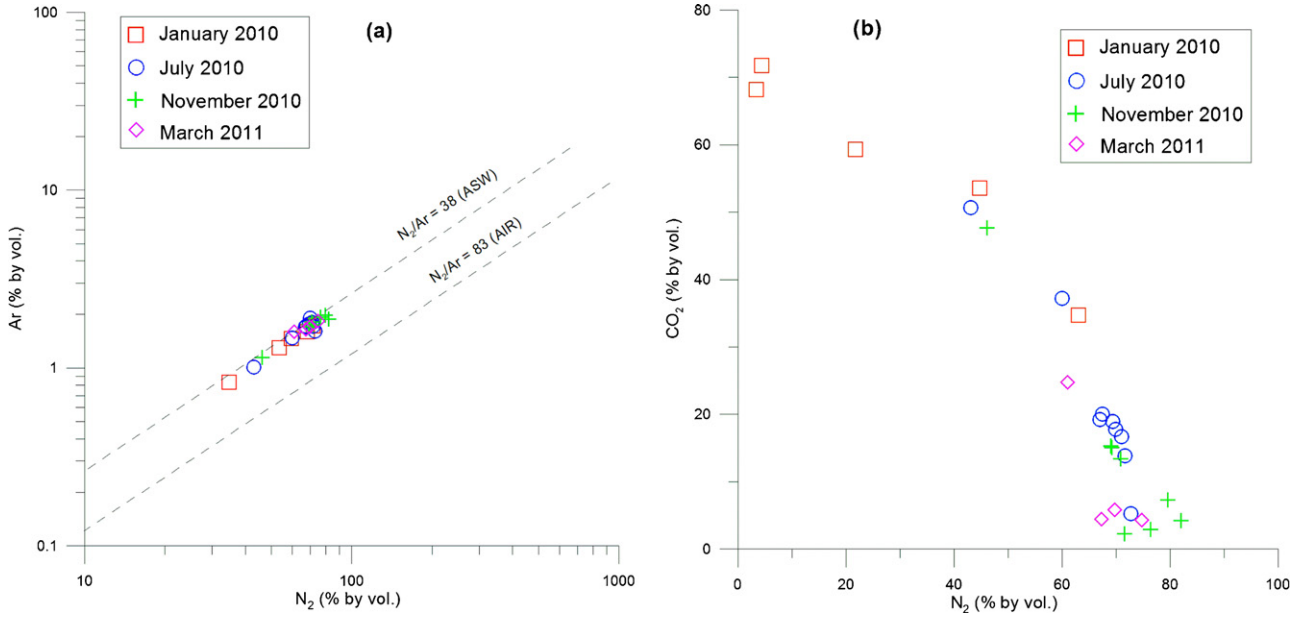

Fig. 7. (a) Argon and (b) CO_2 versus N_2 (in % by vol.) binary diagrams for the dissolved gases in the HH waters.

The amount of carbonic acid is progressively reduced as a consequence of water–rock interaction, which leads to conversion of both carbonic acid to the conjugate base, bicarbonate ion, and the latter to the carbonate ion at higher pH values:

$$H_2CO_3 = HCO_3^- + H^+ \quad K_1 \frac{\left(a_{H+} m_{HCO_3^-} \gamma_{HCO_3^-}\right)}{m_{H_2CO_3^*} \gamma_{H_2CO_3^*}} = 10^{-6.35} \quad 25\,^\circ C \tag{5}$$

$$HCO_3^- = CO_3^{2-} + H^+ \quad K_2 \frac{\left(a_{H+} m_{CO_3^{2-}} \gamma_{CO_3^{2-}}\right)}{m_{HCO_3^-} \gamma_{HCO_3^-}} = 10^{-10.33} \quad 25\,^\circ C \tag{6}$$

Carbonic acid, total bicarbonate (HCO_3^- and related complexes) and total carbonate ion (CO_3^{2-} and related complexes) form the so-called total dissolved inorganic carbon (TDIC).

Conversion of carbonic acid in the conjugate bases during weathering is a process at constant TDIC only in systems closed with respect to $CO_{2(g)}$, that is if no loss/acquisition of gaseous CO_2 occurs toward/from an external reservoir, no carbonate minerals precipitate. In contrast, this process causes an increase in carbonate alkalinity of waters. The same acid-base neutralization process in open system, i.e. under natural conditions of constant supply of gaseous CO_2, implies an increase of both total alkalinity and TDIC, the latter representing, in some way, an index of the compositional evolution of natural waters (e.g. Marini, 2007).

In the pCO_2 and pH binary diagram of Fig. 9 the HH waters are compared with the theoretical curves representing three iso-TDIC concentrations lines (TDIC = 10,100 and 1000 mg HCO_3/L, respectively). As expected, the pCO_2 values show a negative correlation with those of pH, with no variability of the TDIC contents, being the HH waters comprised between 0.0033 and 0.0080 mol/L, suggesting a acid-base neutralization process in closed systems with respect to $CO_{2(g)}$. The partial pressure of CO_2 is between 2.97×10^{-3} to 5.33×10^{-2} bars. The highest pCO_2 values are associated to FH3, FA13 and PDS7, which are characterized by relatively low pH (6.74, 7.16 and 7.49, respectively) values. It is worthwhile to mention that the great majority of the measured and calculated TDIC values (Table 5) are in a narrow range with a difference of 10–15%.

5.5. Isotopic composition of TDIC

The measured and calculated δ^{13}C-TDIC values (Table 4) of the total inorganic carbon dissolved in the HH waters (from −16.9 to −8.5‰) and the low variability of the TDIC contents suggest that inorganic carbon in the HH shallow aquifer is likely derived from the same source. In Fig. 10 the TDIC and δ^{13}C-TDIC values are reported along with the theoretical lines representing the TDIC and δ^{13}C-TDIC evolution of infiltrating water through carbonate terrains where a CO_2 source is active according two different models: (i) addition of soil CO_2 deriving from oxidation of organic matter and root respiration (biogenic), (ii) addition of deeply derived CO_2 and in equilibrium with calcite.

The theoretical curves were computed by means of the EQ3/6 code, starting from low to middle TDIC values, 0.003 and 0.005 mol/kg, respectively, according to Chiodini et al. (2000) and Frondini et al. (2008). In order to investigate the effects of CO_2 on the TDIC and δ^{13}C-TDIC values, the input of CO_2 biogenic was modeled by the addition of 0.01 mol of carbon to infiltrating waters with a δ^{13}C value of −20‰ (V-PDB), whilst the δ^{13}C values of deep CO_2 added to the solution were ranging from −7 (typical of mantle-derived) to 0.0‰ (calcite dissolution). The geochemical modeling that best fit the observed TDIC-δ^{13}C-TDIC composition of the HH waters is reported in Fig. 10. The HH waters are characterized by TDIC <0.008 mol/kg and are generally positioned along the theoretical curves representing the addition of biogenic soil CO_2. Moreover, the pCO_2 values that are higher than the atmospheric average ($10^{-3.5}$ bar), testify a variable contribution to waters of CO_2 produced through biological activity of plants and decomposition/oxidation of organic matter in soils (Appelo and Postma, 1993) that, in oxidized environments, can be expressed through the following simplified reaction:

$$CH_2O + O_2 \rightarrow CO_2 + H_2O \tag{7}$$

where CH_2O stoichiometry closely represents the mean composition of organic matter. Thus, we may conclude that no evidence of a deep-routed CO_2 was highlighted in the HH waters.

Table 5
Saturation index, activity of the main ions and SiO_2, log(pCO_2) and measured and calculated TDIC (in mol/L) for the HH waters.

Sample	Date	Si_{calc}	Si_{dol}	Si_{musc}	SI_{ab}	$SI_{K\text{-}feld}$	SI_{anh}	SI_{gyp}	SI_{an}	SI_{magns}	aCa	aMg	aNa	aK	$aHCO_3$	$aSiO_2$	log(pCO_2)	$TDIC_{meas.}$	$TDIC_{calc.}$
LA1	Jan-10	−0.08	−0.26	−1.04	−3.62	−1.70	−2.64	−2.33	−9.49	−1.90	1.61E-03	9.84E-05	4.36E-04	1.86E-05	3.85E-03	6.54E-05	−1.9	0.0043	0.0050
EV2	Jan-10	0.18	0.39	−0.74	−3.58	−1.07	−3.18	−2.87	−8.98	−1.51	1.48E-03	1.23E-04	1.23E-04	2.10E-05	4.21E-03	9.93E-05	−2.1	0.0047	0.0052
FH3	Jan-10	0.20	0.51	−0.20	−3.63	−0.19	−2.09	−1.76	−9.33	−1.42	2.12E-03	2.13E-04	7.79E-05	1.07E-04	4.69E-03	1.31E-04	−1.9	0.0054	0.0062
FL4	Jan-10	0.38	0.85	−0.78	−3.45	−1.06	−2.71	−2.36	−8.70	−1.27	1.40E-03	1.40E-04	8.37E-05	9.35E-06	3.63E-03	8.28E-05	−2.5	0.0041	0.0043
FP5	Jan-10	−0.18	−0.24	−0.92	−3.91	−1.20	−2.78	−2.47	−9.67	−1.78	1.52E-03	1.53E-04	1.11E-04	3.03E-05	3.93E-03	1.03E-04	−1.8	0.0044	0.0053
EV2	Jul-10	0.10	−0.13	−0.71	−3.62	−1.08	−3.30	−2.99	−9.14	−1.95	1.59E-03	5.73E-05	1.51E-04	2.80E-05	4.07E-03	9.41E-05	−2.0	0.0057	0.0051
FH3	Jul-10	0.25	0.40	−0.27	−2.50	−0.35	−1.93	−1.63	−9.14	−1.56	2.25E-03	1.30E-04	1.31E-03	1.04E-04	5.36E-03	1.43E-04	−1.7	0.0066	0.0072
FL4	Jul-10	0.34	0.44	−0.84	−3.38	−1.03	−2.76	−2.44	−8.70	−1.63	1.63E-03	7.08E-05	1.03E-04	1.16E-05	3.95E-03	1.09E-04	−2.3	0.0050	0.0047
FP5	Jul-10	0.21	0.15	−0.68	−3.39	−0.85	−2.76	−2.47	−8.86	−1.76	1.72E-03	7.02E-05	1.31E-04	2.56E-05	4.08E-03	1.30E-04	−2.1	0.0058	0.0051
FCL6	Jul-10	0.08	0.47	−0.92	−4.02	−1.63	−3.57	−3.29	−8.87	−1.32	1.30E-03	1.95E-04	9.58E-05	1.41E-05	3.80E-03	7.46E-05	−2.1	0.0043	0.0046
PDS7	Jul-10	0.01	0.39	−0.92	−3.37	−1.18	−3.11	−2.79	−9.05	−1.34	1.12E-03	2.07E-04	1.48E-04	1.18E-05	3.25E-03	1.02E-04	−2.3	0.0042	0.0039
RU8	Jul-10	0.81	1.96	0.12	−2.24	−0.19	−2.52	−2.26	−7.29	−0.54	1.47E-03	2.22E-04	4.63E-04	3.48E-05	3.94E-03	1.38E-04	−2.7	0.0052	0.0046
PH9	Jul-10	0.13	0.44	−0.90	−3.84	−1.51	−3.17	−2.86	−8.95	−1.41	1.39E-03	1.59E-04	1.20E-04	1.40E-05	3.89E-03	7.43E-05	−2.1	0.0044	0.0048
RC9	Jul-10	1.06	2.26	0.11	−2.50	−0.53	−2.95	−2.72	−6.80	−0.46	1.48E-03	1.46E-04	3.41E-04	2.32E-05	4.51E-03	1.03E-04	−2.8	0.0059	0.0052
RL10	Jul-10	0.53	0.57	−0.46	−2.41	−0.56	−2.81	−2.52	−8.19	−1.66	1.73E-03	4.20E-05	5.02E-04	2.09E-05	4.08E-03	1.45E-04	−2.4	0.0056	0.0049
AC11	Jul-10	0.09	0.36	−0.91	−3.80	−1.34	−3.17	−2.85	−9.18	−1.45	1.50E-03	1.77E-04	1.11E-04	1.63E-05	3.99E-03	8.30E-05	−2.1	0.0045	0.0050
FA12	Jul-10	0.18	0.20	−1.06	−3.93	−1.69	−3.15	−2.85	−9.04	−1.70	1.63E-03	8.47E-05	1.23E-04	1.16E-05	4.50E-03	7.29E-05	−2.0	0.0059	0.0056
EV2	Nov-10	−0.01	−0.33	−1.03	−3.83	−1.42	−3.23	−2.91	−9.34	−2.04	1.52E-03	5.75E-05	1.19E-04	1.64E-05	4.05E-03	9.31E-05	−1.9	0.0048	0.0052
FH3	Nov-10	−0.21	−0.72	−0.84	−3.29	−1.22	−2.10	−1.84	−9.70	−2.20	2.06E-03	6.96E-05	9.31E-04	7.30E-05	5.13E-03	1.28E-04	−1.3	0.0080	0.0083
FL4	Nov-10	−0.03	−0.35	−1.20	−3.84	−1.51	−2.57	−2.27	−9.27	−2.03	1.64E-03	6.19E-05	9.76E-05	1.16E-05	3.78E-03	1.08E-04	−1.9	0.0047	0.0049
FP5	Nov-10	−0.14	−0.46	−1.18	−3.89	−1.36	−2.63	−2.32	−9.68	−2.04	1.74E-03	8.64E-05	1.02E-04	1.86E-05	4.18E-03	1.17E-04	−1.7	0.0048	0.0058
FCL6	Nov-10	0.16	0.67	−0.96	−3.58	−1.39	−3.36	−3.05	−8.76	−1.21	1.24E-03	2.08E-04	1.10E-04	9.39E-06	3.59E-03	9.09E-05	−2.3	0.0040	0.0043
PDS7	Nov-10	−0.08	0.21	−0.95	−3.36	−1.25	−2.88	−2.55	−9.16	−1.44	1.06E-03	1.92E-04	1.85E-04	1.18E-05	3.02E-03	9.34E-05	−2.3	0.0033	0.0036
RU8	Nov-10	0.31	1.12	0.04	−2.16	0.41	−1.92	−1.58	−8.88	−0.92	1.64E-03	3.96E-04	5.15E-04	8.91E-05	3.81E-03	1.85E-04	−2.3	0.0044	0.0047
PH9	Nov-10	0.01	0.21	−0.89	−4.08	−1.63	−3.06	−2.80	−8.83	−1.48	1.36E-03	1.53E-04	1.03E-04	1.87E-05	3.61E-03	8.16E-05	−2.0	0.0040	0.0045
RL10	Nov-10	0.32	0.21	−0.41	−2.91	−0.72	−2.51	−2.17	−8.88	−1.84	1.95E-03	5.82E-05	4.78E-04	3.47E-05	3.59E-03	8.49E-05	−2.3	0.0044	0.0044
AC11	Nov-10	0.57	1.34	−0.42	−3.32	−0.82	−3.23	−2.91	−8.07	−0.95	1.37E-03	1.66E-04	8.58E-05	1.41E-05	3.66E-03	8.79E-05	−2.7	0.0041	0.0042
FA13	Nov-10	−0.08	−0.19	−1.48	−4.40	−2.09	−4.51	−4.21	−9.47	−1.82	1.51E-03	1.09E-04	6.37E-05	7.01E-06	4.19E-03	7.41E-05	−1.8	0.0048	0.0055
FEA14	Nov-10	0.56	0.47	−0.23	−3.17	−0.62	−2.81	−2.48	−8.33	−1.82	1.62E-03	2.85E-05	1.60E-04	2.80E-05	3.91E-03	8.13E-05	−2.5	0.0044	0.0046
RH15	Nov-10	0.34	0.91	−0.51	−3.39	−0.75	−2.95	−2.61	−8.75	−1.17	1.37E-03	1.83E-04	1.00E-04	2.10E-05	3.99E-03	9.37E-05	−2.4	0.0045	0.0047
RR16	Nov-10	0.63	1.47	−0.07	−2.80	−0.16	−2.72	−2.39	−8.08	−0.89	1.46E-03	1.85E-04	1.41E-04	3.03E-05	3.78E-03	1.17E-04	−2.7	0.0043	0.0044
RUT17	Nov-10	0.27	0.50	0.24	−2.94	0.23	−2.44	−2.10	−8.76	−1.50	1.49E-03	1.08E-04	1.72E-04	1.19E-04	3.18E-03	1.18E-04	−2.5	0.0036	0.0038
EV2	Mar-11	−0.05	−0.48	−1.08	−3.94	−1.54	−2.87	−2.55	−9.61	−2.15	1.72E-03	5.62E-05	1.46E-04	1.86E-05	4.25E-03	7.82E-05	−1.8	0.0067	0.0057
FH3	Mar-11	0.15	−0.08	−0.40	−2.88	−0.48	−2.01	−1.67	−9.66	−1.97	2.33E-03	7.74E-05	7.75E-04	9.08E-05	5.16E-03	1.07E-04	−1.8	0.0078	0.0071
FL4	Mar-11	−0.05	−0.51	−1.46	−4.05	−1.89	−2.56	−2.21	−9.64	−2.20	1.79E-03	5.63E-05	9.91E-05	6.51E-06	3.51E-03	6.93E-05	−2.0	0.0053	0.0046
FP5	Mar-11	−0.07	−0.47	−0.82	−4.08	−1.32	−2.67	−2.35	−9.52	−2.12	1.76E-03	6.27E-05	1.11E-04	3.37E-05	3.95E-03	7.99E-05	−1.8	0.0064	0.0053
FCL6	Mar-11	0.06	0.34	−1.06	−3.90	−1.53	−3.13	−2.80	−9.23	−1.45	1.37E-03	1.79E-04	9.17E-05	1.03E-05	3.66E-03	7.24E-05	−2.2	0.0062	0.0045
PDS7	Mar-11	−0.63	−0.89	−1.45	−3.93	−1.67	−3.64	−3.29	−10.56	−2.00	1.22E-03	2.32E-04	1.96E-04	1.64E-05	3.35E-03	9.14E-05	−1.6	0.0042	0.0051
RU8	Mar-11	−0.25	−0.26	−1.09	−3.45	−1.25	−2.17	−1.80	−10.24	−1.77	1.71E-03	2.39E-04	3.81E-04	2.46E-05	3.92E-03	8.27E-05	−1.8	0.0050	0.0056
PH9	Mar-11	−0.01	0.11	−1.13	−4.09	−1.77	−2.90	−2.59	−9.30	−1.60	1.47E-03	1.54E-04	1.07E-04	1.17E-05	3.80E-03	6.76E-05	−2.0	0.0055	0.0048
RC9	Mar-11	0.08	0.25	−0.66	−3.35	−1.18	−2.53	−2.21	−9.27	−1.56	1.62E-03	1.52E-04	4.40E-04	3.33E-05	4.13E-03	7.51E-05	−2.0	0.0049	0.0052
RL10	Mar-11	0.27	−0.02	−0.61	−3.17	−1.20	−2.52	−2.19	−8.98	−2.03	1.83E-03	3.93E-05	5.53E-04	2.48E-05	3.86E-03	6.36E-05	−2.2	0.0051	0.0047
AC11	Mar-11	−0.14	−0.13	−1.09	−4.04	−1.51	−2.99	−2.68	−9.47	−1.71	1.50E-03	1.61E-04	9.12E-05	1.64E-05	3.53E-03	8.93E-05	−1.9	0.0051	0.0046
FA13	Mar-11	−0.43	−1.05	−1.87	−4.76	−2.46	−3.07	−2.75	−10.31	−2.35	1.68E-03	8.32E-05	6.74E-05	6.98E-06	4.20E-03	6.98E-05	−1.5	0.0056	0.0067
RR16	Mar-11	0.52	1.37	−0.33	−2.93	−0.41	−2.62	−2.26	−8.61	−0.89	1.61E-03	2.88E-04	1.59E-04	2.30E-05	3.86E-03	9.69E-05	−2.6	0.0069	0.0046
RUT17	Mar-11	0.56	0.86	−0.50	−2.98	−0.87	−2.41	−2.03	−8.69	−1.46	1.87E-03	8.58E-05	3.08E-04	1.62E-05	3.83E-03	6.28E-05	−2.6	0.0054	0.0045
RCM18	Mar-11	0.34	0.86	−0.30	−3.00	−0.77	−2.48	−2.15	−8.75	−1.21	1.64E-03	1.91E-04	4.81E-04	4.09E-05	3.98E-03	7.65E-05	−2.3	0.0051	0.0048
EV2	Apr-11	−0.10	−0.67	−1.11	−3.39	−0.78	−3.01	−2.58	−10.42	−2.36	1.81E-03	5.45E-05	1.34E-04	1.77E-05	4.17E-03	9.99E-05	−2.0	n.d.	n.d.
RL10	Apr-11	0.40	0.15	−0.59	−3.01	−1.02	−2.59	−2.27	−8.71	−1.97	1.88E-03	3.33E-05	4.34E-04	2.13E-05	4.04E-03	8.04E-05	−2.3	n.d.	n.d.
FH3	Apr-11	0.12	−0.72	−0.48	−2.73	−0.43	−1.94	−1.61	−9.70	−2.58	2.44E-03	2.01E-05	9.13E-04	8.90E-05	5.45E-03	1.33E-04	−1.7	n.d.	n.d.
FP5	Apr-11	0.01	−0.30	−1.06	−3.85	−1.39	−2.59	−2.27	−9.40	−2.02	1.92E-03	7.11E-05	1.20E-04	1.85E-05	4.04E-03	9.94E-05	−1.9	n.d.	n.d.

calc: calcite; dol: dolomite; musc: muscovite; ab: albite; K-feld: K-feldspar; any: anhydrite; gyp: gypsum; mangs: magnesite.

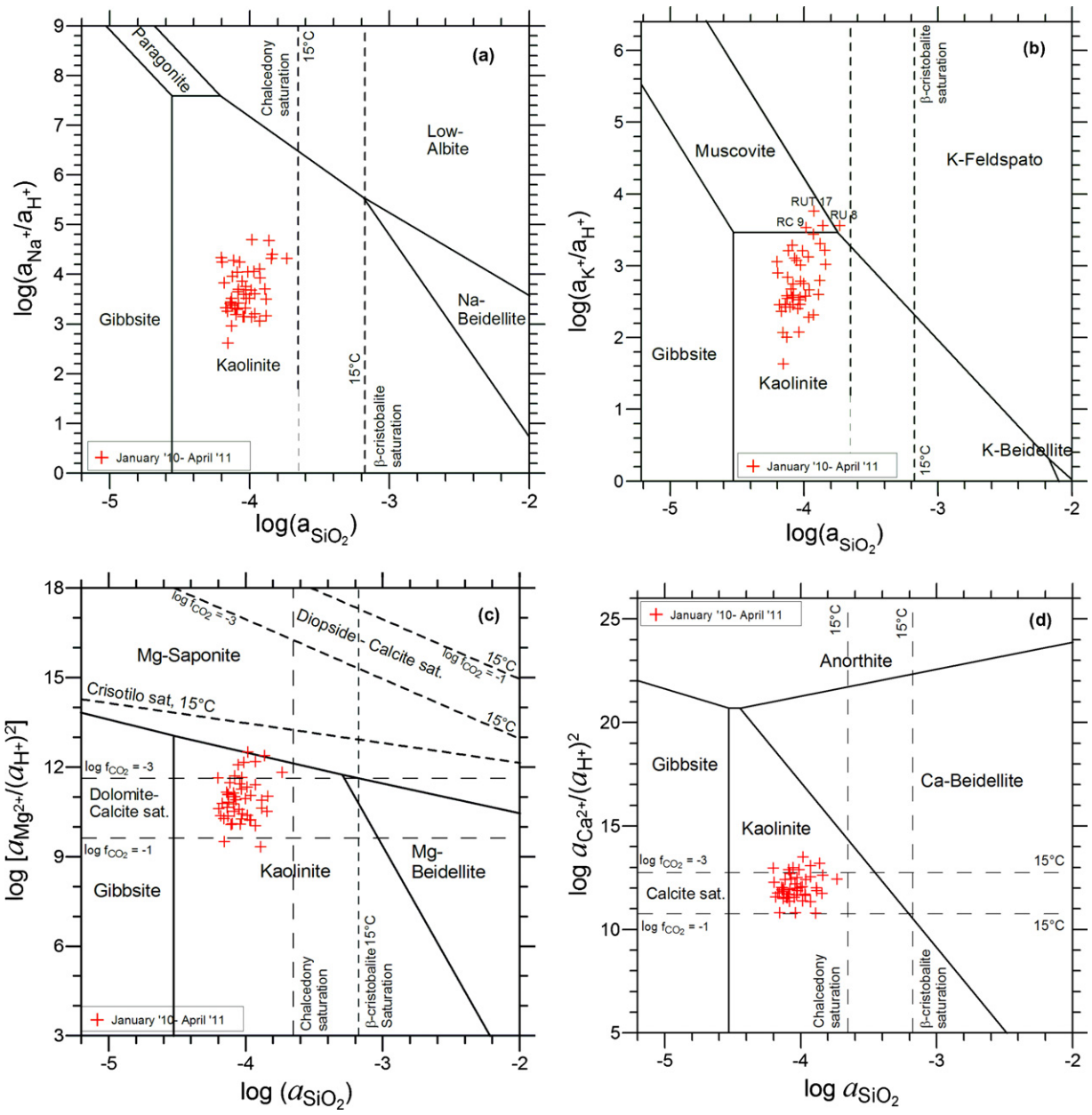

Fig. 8. Activity plots for the (a) Na_2O-SiO_2-Al_2O_3-H_2O, (b) K_2O-SiO_2-Al_2O_3-H_2O, (c) MgO-SiO_2-Al_2O_3-H_2O and (d) CaO-SiO_2-Al_2O_3-H_2O systems at 15 °C, 1.013 bar. Saturation lines for quartz and amorphous silica are also reported. The saturation lines for calcite and dolomite correspond to $logf_{CO_2}$ of −1 and −3, respectively.

5.6. Implications for the water and dissolved gas geochemical monitoring

The HH area can be considered suitable for CO_2 storage since the injection will be located in a 3 km × 5 km dome-shape structure (Alcalde et al., 2010) where porous and permeable aquifers hosted in Lower Jurassic carbonate and dolomite beds occur at about 1500 m depth. The overlying marl strata are a potential cap rock, while anhydrites can be regarded as a lower seal. The thermal gradient in the area, derived by the oil wells, has a mean value of 26 °C/km (Fernàndez et al., 1998). The integrity of the cap rock once CO_2 will be injected is also apparently guaranteed by the low seismicity affecting this area. In fact, according to the National Institute of Geography, from 1939 to 2011

Table 6
Maximum, minimum and mean values (in mg/L) of the main chemical parameters of the HH brines.

	Temp.	pH	Na	K	Ca	Mg	HCO_3	Cl	SO_4	TDS	Salinity
Mean	21.6	7.3	8832	431	1676	773	244	17,390	1782	31,129	26,222
Min	21.0	6.7	6312	276	1089	338	24	11,797	1058	20,894	18,109
Max	22.6	9.3	10,384	536	2058	1004	367	20,840	2242	37,432	31,224

Source: By courtesy of A. Perez Estuan.
TDS: Total Dissolved Solids; salinity as NaCl (in mg/L).

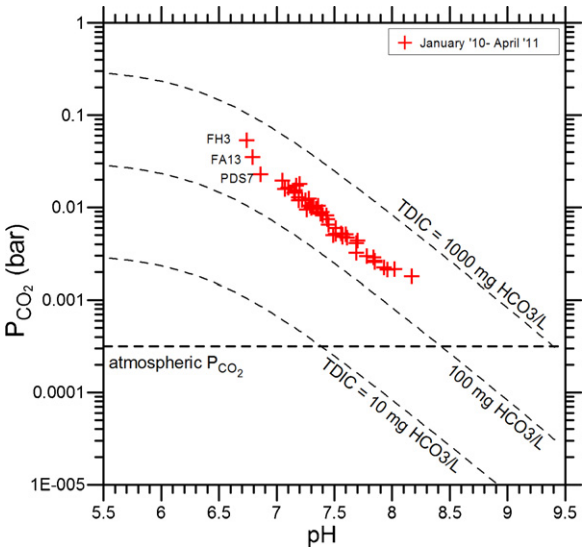

Fig. 9. pCO_2 versus pH binary diagram for HH waters. The theoretical curves representing three iso-TDIC concentrations lines (TDIC = 10, 100 and 1000 mg HCO_3/L, respectively) are also reported.

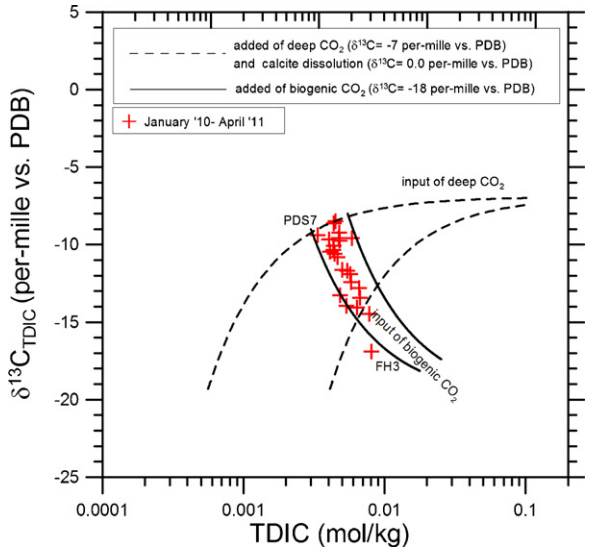

Fig. 10. Total Dissolved Solids (TDIC) vs. δ^{13}C-TDIC for the HH waters. Solid and dash lines represent the theoretical trends related to the input of deep and biogenic CO_2. The HH water samples are clearly associated with a biogenic source.

about fifteen >2.0 M seismic events were recorded (http://www.ign.es/ign/layoutIn/sismoTerremotosEspana.do?value=2) in the Burgos region, the highest magnitude being recorded in 1939 (4.3 M). Nevertheless, in this span of time at HH only one significant event occurred NW of Huermeces with a magnitude of 2.3 M.

These features suggest that CO_2 can safely be injected. However, the HH area is interested by a main structure, namely the Ubierna-Ventaniella fault system (e.g. Tavani, 2012) (Fig. 1). It formed the southern boundary of the Baque-Cantabrian Basin in the Late Jurassic-Early Cretaceous (e.g. Rat, 1988) along with NE-SW striking and NW dipping faults (Tavani and Anton Muñoz, 2012). This structure may act as a permeable zone favoring the fluids uprising if a CO_2 leakage would occur through the cap rock. Similarly, other fracture or fault systems, covered by the Quaternary sediments, can be present in the proximity of the oil wells (Fig. 1), the latter potentially being leakage points. This would apparently explain the presence of possible contribution by deeper waters in some springs (e.g. samples FH3 and FL4) fed by the shallow hydrological circuits and surface waters (RU8).

The maximum, minimum and mean values (11 samples collected in 2010) of the main solutes measured from the H-2 well brine, kindly provided by A. Perez Estuan and described in a technical report of CIEMAT (Barcelona, Spain) by Buil et al. (2012), are listed in Table 6. The brine has a salinity is 26 g/L (as NaCl) and a slightly alkaline pH value (7.3). The Cl/SO_4 molar ratio is about 26 and strongly differs of about one order of magnitude with respect to those calculated in the studied waters, similarly to other molar ratios less affected by secondary processes (e.g. salt precipitation), such as Na/K and Mg/Cl. Despite the fact that no trace elements are available for the HH brine, on the basis of the sole main solutes any brine leakage to the surface should be detected. However, it has to be considered that the injection of CO_2 (in the case of HH less than 100,000 tons will be injected with a purity >99%) may induce the formation of a CO_2 plume. According to Chadwick et al. (2005), less than 1000 tons of CO_2 should be detectable at depths of less than 1000 m by seismic methods. In near-surface environments, such as ground waters, CO_2 flow should be migrating as bubbles in fault systems and/or near borehole. Thus, we may speculate that the equilibrium of the carbonate species should first be modified causing an acidification of the shallow waters and the increase of HCO_3^- (e.g. Myrttinen et al., 2012 and references therein) and free-CO_2. Consequently, the dolomite and calcite saturation lines reported in Fig. 8c–d are of special interest for the geological sequestration of CO_2. In the case of a CO_2 leakage, the shallow aquifers may increase $\log f_{CO_2}$, probably modifying the geochemical barrier reported in Fig. 8c–d.

This process is also expected to affect the carbon isotopic composition of TDIC and dissolved CO_2. The industrial CO_2 to be injected in a pilot site is indeed usually derived by refinery gas processing and the δ^{13}C-CO_2 values are rather negative, e.g. from to −36 (Vaselli, unpublished data) to −28‰ V-PDB as that used in the Ketzin pilot site, e.g. Myrttinen et al. (2010). The isotopic and geochemical data of TDIC (e.g. Barth et al., 2003) and dissolved CO_2 may allow to distinguish different sources, e.g. atmosphere, soil respiration, carbonate. Thus, the isotopic and chemical equilibrium of the C-bearing inorganic species can be used to trace CO_2 leakage if the injected CO_2 would have an isotopic carbon ratio that differs with respect to that already present (Raistrick et al., 2006). The δ^{13}C-CO_2 values measured in the HH waters are clustering around −20‰ V-PDB and thus are more positive than those of the injected CO_2 at Ketzin. Nevertheless, if we consider that the baseline of δ^{13}C-TDIC of the HH shallow aquifer has a value −10‰ V-PDB (Table 4), i.e. similar to other aquifers worldwide (e.g. Clark and Fritz, 1997), the injection of CO_2 with a carbon isotopic value of −30‰ V-PDB should decrease the δ^{13}C-TDIC to more negative values than those observed. By simulating the addition of 100 steps of 0.01 mol of CO_2 (δ^{13}C-CO_2 = −30‰ V-PDB and δ^{13}C-TDIC = −10‰ V-PDB) and considering the maximum (0.008 mol/kg), minimum (0.0033 mol/kg) and mean (0.0052 mol/kg) TDIC values of the HH waters, the resulting δ^{13}C-TDIC and TDIC values would indeed be −28.6‰ and 0.12 mol/kg, −29.4‰ and 0.11 mol/kg, and −29.1‰ and 0.11 mol/kg, respectively.

It is to point out that the injection and the leakage rates (not yet established), if occurring, are critical factors for modifying the present chemical features of the studied system. Furthermore, the isotopic composition of the CO_2 in the HH brine is not known and thus, it is not possible to compare the injected CO_2 with that present at depth.

Summarizing, the establishment of the geochemical baseline of surface and ground waters through monitoring programs, that should include the acquisition of large spectrum of chemical and isotopic parameters, before commencing the pre-injection of CO_2

is a key point for assuring that during the operational and post-operational period no modifications have occurred.

6. Conclusions

In this paper the very first geochemical and isotopic data for the surface and spring waters from the HH, where a pilot plant will shortly be established to inject pure CO_2, were presented. The chemical and isotopic compositions indicate that the studied waters, characterized by relatively low TDS and a $Ca^{2+}(Mg^{2+})$-HCO_3^- hydrochemical facies, are fed by meteoric waters circulating along a shallow hydrogeological pattern. Despite the fact that an anthropogenic source of NO_3 was recognized, two springs (namely Fuente Hontomin: FH3 and, at minor extent, Fuente Laguillo: LA1) show clues of a possible contribution by deeper waters as derived by the relatively high concentrations of As, B, Ba and U. Similar geochemical features were also found in the Rio Ubierna for which inputs by more saline waters can be hypothesized. The HH water chemistry is mainly related to water–rock interaction processes that involve the sedimentary units characterizing the HH area, such as dissolution of Ca(Mg)-carbonates driven by conversion of H_2CO_3 in HCO_3^- ion. Thus, calcite is the main Ca-supplier, due to its very high dissolution rate, under far-from-equilibrium conditions, compared to that of Ca-bearing silicates and Al-silicates (e.g. Marini, 2007). The $Ca^{2+}(Mg^{2+})$-HCO_3^- waters are indeed generally compatible with closed-system equilibration with carbonate minerals. A significant anthropogenic contamination seems to affect the HH waters, since particularly high NO_3^- concentrations were found in the springs close to the injection area. The $\delta^{13}C$-CO_2 and $\delta^{13}C$-TDIC indicates a biogenic source for carbon dioxide, which in some cases is the dominant component among the dissolved gases, the latter being commonly characterized atmospheric-derived N_2, O_2 and Ar.

The periodical monitoring (from January 2010 to April 2011) carried out in five spring discharges located in the proximity of the site where CO_2 will be injected have indicated significant variations in terms of absolute concentrations and molar ratios of the main components.

The geochemical and isotopic data of the surface and spring waters in the surroundings of HH are relevant since they can be considered as background values when intra- and post-injection monitoring programs will be carried out. As a consequence, main and minor solutes, including the carbonate equilibria, are to be considered if a CO_2 leakage through the cap rock would be occurring. Nevertheless, the recorded presence of an anthropogenic contribution cannot be neglected when computing the effects deriving by a CO_2 leakage whenever would be interacting with the shallow aquifer. Trace elements, particularly for those water samples where a deep component was likely be recognized (e.g. FH3, LA1 and Rio Ubierna), appear also suitable for a geochemical monitoring. Nevertheless, chemistry of the dissolved gases, the geochemical modeling and TDIC and $\delta^{13}C_{TDIC}$ values were also revealed to be important tracers and should be considered when a geochemical monitoring will be designed. The geochemical conditions currently established would indeed change in an event of CO_2 leaking and be recorded in the shallow groundwater system, modifying the geochemical processes governing the water and dissolved gas composition recognized during this pre-injection phase.

Acknowledgments

F. Grandia and J. Bruno are gratefully thanked for their encouragement and help. J. Caballero is gratefully acknowledged for his assistance in the field. Many thanks are due to A. Perez Estaun for kindly providing the unpublished chemical data of the HH brine. This work was financially supported by Fundación Ciudad de la Energía in the framework of a project with the CNR-IGG of Florence (Italy) (Resp. O. Vaselli) and co-financed by the European Community European Energy Programme for Recovery. Many thanks are due to J.J. Gale and three anonymous reviewers who greatly improved an early version of the manuscript.

The sole responsibility of this publication lies with the authors. The European Union is not responsible for any use that may be made of the information contained therein.

References

Alcalde, J., Carbonell, R., Martí, D., Calahorrano, A., Palomeras, I., Ayarza, P., Pérez-Estaún, A., 2010. Seismic characterization of a CO_2 storage pilot plant in a Saline Aquifer (Hontomín, Spain). American Geophysical Union, Fall Meeting 2010. abstract #NS41A-1505.

Appelo, C.A.J., Postma, D., 1993. Geochemistry, Groundwater and Pollution. A.A. Balkema, Rotterdam, 536 pp.

Arostegui, J., Irabien, M.J., Sangüesa, J., Zuluaga, M.C., 2000. La formacion de Utrillas en el borde sur de la Cuenca Vasco-Cantabrica: aspectos estratigraficos, mineralogicos y geneticos. Estudios Geológicos 56, 251–267.

Barth, J.A.C., Cronin, A.A., Dunlop, J., Kalin, R.M., 2003. Influence of carbonates on the riverine carbon cycle in an anthropogenically dominated catchment basin: evidence from major elements and stable carbon isotopes in the Lagan River (N. Ireland). Chemical Geology 200, 203–216.

Benito-Calvo, A., Perez-Gonzalez, A., 2007. Erosion surfaces and Neogene landscape evolution in the NE Duero Basin (north-central Spain). Geomorphology 88, 226–241.

Berner, E.K., Berner, R.A. (Eds.), 1996. Global Environmental: Water, Air and Geochemical Cycles. Prentice-Hall, Upper Saddle River, NJ.

Bowers, T.S., Jackson, K.J., Helgeson, H.C., 1984. Equilibrium activity diagrams for coexisting minerals and aqueous solutions at pressures and temperatures to 5 kb and 600 °C. Springer, New York, pp. 397.

Buil, B., Gómez, P., Peña, J., Garralón, A., Galarza, C., Durán, J.M., Domínguez, R., Escribano, A., Turrero, M.J., Robredo, L.M., Sánchez, L., 2012. Caracterización y monitorización hidrogeoquímica de los acuíferos superiores a la formación almacenamiento de CO_2 (Hontomín, Burgos) y actualización de la caracterización de aguas superficiales. Informe técnico CIEMAT/DMA/2G010/1/2012 (In Spanish).

Calvo, J.M., 2002. Caracterización del valor fertilizante y posible utilización de aguas residuales del proceso de fabricación de explosivos en el Páramo de Masa. Master Thesis in Environmental Engineering. University of Santiago Spain) (In Spanish).

Cantucci, B., Montegrossi, G., Vaselli, O., Tassi, F., Quattrocchi, F., Perkins, E.H., 2009. Geochemical modeling of CO_2 storage in deep reservoirs: the Weyburn Project (Canada) case study. Chemical Geology. 265, 181–197, http://dx.doi.org/10.1016/j.chemgeo.2008.12.029.

Chadwick, R.A., Arts, R., Eiken, O., 2005. 4D seismic quantification of a growing CO_2 plume at Sleipner, North Sea. Petroleum Geology Conference Series 6, 1385–1399.

Clark, I.D., Fritz, P., 1997. Environmental Isotopes in Hydrogeology. Lewis, Boca Raton.

Coleman, M.L., Shepherd, T.J., Rouse, J.E., Moore, G.R., 1982. Reduction of water with zinc for hydrogen isotope analysis. Analytical Chemistry 54, 993–995.

Craig, H., 1961. Isotopic variations in meteoric waters. Science 133, 1702–1703.

Chiodini, G., Frondini, F., Cardellini, C., Parello, F., Peruzzi, L., 2000. Rate of diffuse carbon dioxide Earth degassing estimated from carbon balance of regional aquifers: the case of central Apennine, Italy. Journal of Geophysical Research 105, 8423–8434.

Damen, K., Faaij, A., Turkenburg, W., 2006. Health, safety and environmental risks of underground CO_2 storage—overview of mechanisms and current knowledge. Climatic Change 74, 289–318.

Drever, J.I., 1997. The Geochemistry of Natural Waters – Surface and Groundwater Environments. Prentice Hall, New Jersey, USA, pp. 208.

Epstein, S., Mayeda, T.K., 1953. Variation of the $^{18}O/^{16}O$ ratio in natural waters. Geochimica Cosmochimca Acta 4, 213–224.

Evans, White, W.C., Rapp, L.D., 1998. Geochemistry of some gases in hydrothermal fluids from the southern Juan de Fuca ridge. Journal of Geophysical Research 15, 305–313.

Fernàndez, M., Marzán, I., Correia, A., Ramalho, E., 1998. Heat flow, heat production, and lithospheric thermal regime in the Iberian Peninsula. Tectonophysics 291, 29–53.

Frondini, F., Caliro, S., Cardellini, C., Chiodini, G., Morgantini, N., Parello, F., 2008. Carbon dioxide degassing from Tuscany and Northern Latium (Italy). Global and Planetary Change 61, 89–102.

Gaillardet, J., Dupré, B., Allègre, C.J., Négrel, P., 1997. Chemical and physical denudation in the Amozon River Basin. Chemical Geology 142, 141–173.

Gaillardet, J., Dupré, B., Louvat, P., Allegre, C.J., 1999. Global silicate weathering and CO_2 consumption rates deduced from the chemistry of large rivers. Chemical Geology 159, 3–30.

Gat, J.R., Carmi, H., 1971. Evolution of the isotopic composition of atmospheric waters in the Mediterranean Sea area. Journal of Geophysical Research 75, 3039–3040.

Giggenbach, W.F., 1995. Composition of fluids in geothermal systems of the Taupo Volcanic Zone, New Zealand, as a function of source magma. In: Chudaev, K.A. (Ed.), Water–Rock Interaction, vol. 8, pp. 9–12.
Gunter, W.D., Perkins, E.H., McCann, T.J., 1993. Aquifer disposal of CO_2-rich gases: reaction design for added capacity. Energy Conversion and Management 34, 941–948.
Gunter, W.D., Wiwchar, B., Perkins, E.H., 1997. Aquifer disposal of CO_2-rich gases: extension of the time scale of experiment for CO_2-sequestering reactions by geochemical modeling. Mineralogy and Petrology 59, 121–140.
Gunter, W.D., Perkins, E.H., Hutcheon, I., 2000. Aquifer disposal of CO_2-rich gases: modeling of water–rock reactions for trapping of acid wastes. Applied Geochemistry 15, 1085–1095.
Gunter, W.D., Bachu, S., Benson, S.M., 2004. The role of hydrogeological and geochemical trapping in sedimentary basins for secure geological storage for carbon dioxide. In: Baines, S.J., Worden, R.H. (Eds.), Geological Storage of Carbon Dioxide, vol. 233. Geological Society Special Publication, London, UK, pp. 129–145.
Han, G., Liu, C.-Q., 2004. Water geochemistry controlled by carbonate dissolution: a study of the river waters draining karst-dominated terrain, Guizhou Province, China. Chemical Geology 204, 1–21.
Helgeson, H.C., 1968. Evaluation of irreversible reactions in geochemical processes involving minerals and aqueous solutions: I. Thermodynamic relations. Geochimica Cosmochimica Acta 32, 853–877.
Hernaiz, P.P., 1994. La falla Ubierna (margen SO de la cuenca Cantábrica). Geogazeta 16, 39–42 (In Spanish with English Abstract).
Hernaiz, P.P., Serrano, A., Malagon, J., Rodriguez Canas, C., 1994. Evolucion structural del margen SO de la Cuenca Vasco-Cantabrica. Geogaceta 15, 143–146.
IPCC, 2005. IPCC special report on carbon dioxide capture and storage. In: Metz, B., Davidson, O., de Coninck, H.C., Loos, M., Meyer, L.A. (Eds.), Prepared by Work ing Group III of the Intergovernmental Panel on Climate Change. Cambridge University Press, Cambridge, United Kingdom/New York, NY, USA, p. 442.
ITGE-Instituto Tecnológico GeoMinero de España 1998. Diputación Provincial de Burgos, 1998. Atlas del medio hídrico de la provincia de Burgos.
Jones, D.J., Beaubien, S.E., Baubron, J.C., Cinti, D., Davis, J.R., Emery, C., Fascetti, A., Lombardi, S., Michel, K., Morgantini, N., Penner, L., Quattrocchi, F., Strutt, M.H., 2006. Continued Soil Gas Monitoring at the Weyburn Unit in 2004. Report No. COAL R288 DTI/Pub URN 05/1261, p. 20.
Korre, A., Imrie, C.E., May, F., Beaubien, S.E., Vandermeijer, V., Persoglia, S., Golmen, L., Fabriol, H., Dixon, T., 2011. Quantification techniques for potential CO_2 leakage from geological storage sites. Energy Processes 4, 3413–3420.
Kreamer, D.K., Hodge, V.F., Rabinowitz, I., Johannesson, K.H., Stetzenbach, J., 1996. Trace element geochemistry in water from selected springs in Death Valley National Park, California. Ground Water 34, 95–103.
Langelier, W., Ludwig, H., 1942. Graphical methods for indicating the mineral character of natural waters. Journal of American Water Works Association 34, 335–352.
Lupion, M., Diego, R., Loubeau, L., Navarrete, B., 2011. CIUDEN CCS project: status of the CO_2 capture technology development plant in power generation. Energy Procedia 4, 5639–5646.
Macías, F., Bao, M., Rodríguez, L., Castresana, J.M., Allué, C., Garzía-López, J.M., 2005. Procesos de regeneración de suelos y sistemas forestales en parameras calizas. Ensayos en el Páramo de Masa (Burgos). Proceed. 4th Congress on Spanish Forsts, 26-30 Septiembre 2005. Zaragoza, Spain (In Spanish).
Marini, L., 2007. Geological sequestration of carbon dioxide: thermodynamics, kinetics, and reaction path modeling. In: Developments in Geochemistry. Elsevier Science, Amsterdam, p. 453.
Mediavilla, R., Dabrio, C.J., Martin-Serrano, A., Santisteban, J.L., 1996. Lacustrine Neogene systems of the Duero Basin: evolution and controls. In: Friend, P.F., Dabrio, C.J. (Eds.), Tertiary Basins of Spain: the Stratigraphic Record of the Crustal Kinematics. Cambridge University Press, UK, pp. 228–236.
Meybeck, M., 1979. Concentrations de eaux fluviales en èlèments majeurs et apports en solution aux ocèans. Rev. Gèol. Dyn. Gèogr. Phys. 21, 215–246.
Minissale, A., Vaselli, O., 2011. Karst springs as natural pluviometers: constraints on the isotopic composition of rainfall in the Apennines of central Italy. Applied Geochemistry 26, 838–852.
Myrttinen, A., Becker, V., van Geldern, R., Würdemann, H., Morozova, D., Zimmer, M., Taubald, H., Blum, P., Barth, J.A.C., 2010. Carbon and oxygen isotope indications for CO_2 behaviour after injection: First results from the Ketzin site (Germany). International. Journal of Greenhouse Gas Control 4, 1000–1006.
Myrttinen, A., Becker, Barth, J.A.C., 2012. A review of methods used for equilibrium isotope fractionation investigations between CO2 and dissolved inorganic carbon. Earth Science Reviews 115, 192–199, http://dx.doi.org/10.1016/j.earscirev.2012.08.004.
Mook, W.G., Bommerson, J.C., Staverman, W.H., 1974. Carbon isotope fractionation between dissolved bicarbonate and gaseous carbon dioxide. Earth Planetary. Science Letters 22, 169–176.
Négrel, Ph, Allegre, C.J., Dupre, B., Levin, E., 1993. Erosion sources determined by inversion of major and trace element ratios and strontium isotopic ratios in river water: the Congo Basin case. Earth and Planetary. Science Letters 120, 59–76.
Oldenburg, C.M., 2003. Carbon dioxide as cushion gas for natural gas storage. Energy & Fuels 17, 240–246.
Permanyer, A., Márquez, G., Gallego, J.R., 2013. Compositional variability in oils and formation waters from the Ayoluengo and Hontomín fields (Burgos, Spain). Implications for assessing biodegradation and reservoir compartmentalization. Organic Geochemistry 54, 125–139.
Pruess, K., García, J., 2002. Multiphase flow dynamics during CO_2 injection into saline aquifers. Environmental Geology 42, 282–295.
Quesada, S., Dorronsoro, C., Robles, S., 1995. Genetic relationship between the oil of the Ayoluengo field and the Liassic source-rock of the Southwestern Basque-Cantabrian Basin (Northern Spain). In: Edited by Grimalt, J.O., Dorronsoro, C. (Eds.), Organic Geochemistry: Developments and Applications to Energy, Climate, Environment and Human History. A.I.G.O.A., Donostia-San Sebastian, p. 461463.
Quesada, S., Dorronsoro, C., Robles, S., Chaler, R., Grimalt, J.O., 1997. Geochemical correlation of oil form the Ayoluengo field to Liassic black shale units in the southwestern Basque-Cantabrian Basin (northern Spain). Organic Geochemistry 27, 25–40.
Quesada, S., Robles, S., 1995. Organic geochemistry, distribution and depositional dynamics of the Liassic or- ganic facies of the Basque-Cantabrian Basin (Northern Spain). In: Grimalt, J.O., Dorronsoro, C. (Eds.), Organic Geochemistrw Developments and Applications to Energy, Climate, Environment and Human History. A.1.G.O.A, Donostia- San Sebastian, pp. 464–465.
Quesada, S., Robles, S., Pujalte, V., 1993. E1 Jurásico marino del margen suroccidental de la Cuenca Vasco-Cantábrica y su relación con la explotación de hidrocarburos. Geogaceta 13, 92–96.
Quintá, A., Tavani, S., 2012. The foreland deformation in the south-western Basque-Cantabrian Belt (Spain). Tectonophysics 576-577, 4–19.
Raistrick, M., Mayer, B., Shevalier, M., Perez, R.J., Hutcheon, I., Perkins, E., Gunter, B., 2006. Using chemical and isotopic data to quantify ionic trapping of injected carbon dioxide in oil field brines. Environmental Science & Technology 40, 6744–6749.
Rat, P., 1988. The Basque–Cantabrian Basin between the Iberian and European plates some facts but still many problems. Revista de la Sociedad. Geológica de España 1, 327–348.
Rollinson, H., 1993. Using Geochemical Data. Longman, London, UK, pp. 352.
Roy, S., Gaillardet, J., Allègre, C.J., 1999. Geochemistry of dissolved and suspended loads of the Seine river, France: anthropogenic impact, carbonate and silicate weathering. Geochimica et Cosmochimica Acta 63, 1277–1292.
Rutqvist, J., Tsang, C.-F., 2002. A study of caprock hydromechanical changes associated with CO_2 injection into a brine aquifer. Environmental Geology 42, 296–305.
Salata, G.G., Roelke, L.A., Cifuentes, L.A., 2000. A rapid and precise method for measuring stable carbon isotope ratios of dissolved inorganic carbon. Marine Chemistry 69, 153–161.
Santisteban, J.L., Mediavialla, R., Martin-Serrano, A., Dabrio, C.J., 1996. In: Friend, P.F., Dabrio, C.J. (Eds.), Tertiary Basins of Spain: the Stratigraphic Record of the Crustal Kinematics. Cambridge University Press, UK, pp. 183–187.
Sanchez-Moya, Y., Sopena, A., 2004. El Rift Mesozoico Iberico. In: Vera, J.A. (Ed.), Geologia de Espana, Sociedad. Geológica de Espana. IGME, Madrid, pp. 484–485.
Serrano-Oñate, A., Martínez del Olmo, W., Cámara Rupelo P., 1990. Diapirismo del Trías salino en el Dominio Cántabro-Navarro. In Libro Homenaje a Rafael Soler: Asociación de Geólogos y Geofísicos del Petróleo, pp. 115–122 (In Spanish).
Solomon, S., Carpenter, M., Flach, T.A., 2008. Intermediate storage of carbon dioxide in geological formations: a technical perspective. International Journal of Greenhouse Gas Control 2, 502–510.
Stumm, W., Morgan, J.J., 1996. Aquatic Chemistry. Chemical Equilibrium and Rates in Natural Waters. New York, John Wiley.
Tassi, F., Montegrossi, G., Vaselli, O., 2004. Metodologie di campionamento ed analisi in fase gassosa. CNR-IGG Florence, Internal Report 1/2004, pp. 17 (in Italian).
Tassi, F., Vaselli, O., Luchetti, G., Montegrossi, G., Minissale, A., 2008. Metodo per la determinazione dei gas disciolti in acque naturali. CNR-IGG Rapporto Interno n. 2/2008, pp. 10 (in Italian).
Tassi, F., Vaselli, O., Tedesco, D., Montegrossi, G., Darrah, T., Cuoco, E., Mapendano, M.Y., Poreda, R., Delgado Huertas, A., 2009. Water and gas chemistry at Lake Kivu (DRC): geochemical evidence of vertical and horizontal heterogeneities in a multi-basin structure. Geochemistry, Geophysics, Geosystems 10 (2), http://dx.doi.org/10.1029/2008GC002191.
Tavani, S., Anton Muñoz, J., 2012. Mesozoic rifting in the Basque–Cantabrian Basin (Spain): inherited faults, transversal structures and stress perturbation. Terra Nova, http://dx.doi.org/10.1111/j. 1365-3121.2011.01040x.
Tavani, S., Quintà, A., Granado, P., 2011. Cenozoic right-lateral wrench tectonics in the Western Pyrenees (Spain): the Ubierna Fault System. Tectonophysics 509, 238–253.
Vaselli, O., Tassi, F., Montegrossi, G., Capaccioni, B., Giannini, L., 2006. Sampling and analysis of volcanic gases. Acta Vulcanologica 18, 65–76.
Voltattorni, N., Caramanna, G., Cinti, D., Galli, G., Pizzino, L., Quattrocchi, F., 2006. Study of CO_2 natural emissions in different Italian geological scenarios: refinement of natural hazard and risk assessment. In: Lombardi, S., Altunina, K.L., Beaubien, S.E. (Eds.), Advances in Geological Storage of Carbon Dioxide. NATO Science Series. Springer Publishing, Berlin, pp. 175–190.
Widory, D., Petelet-Giraud, E., Négrel, P., Ladouche, B., 2005. Tracking the sources of nitrate in groundwater using coupled nitrogen and boron isotopes: a synthesis. Environmental Science & Technology 39, 539–548.
Wolery, T.W., Jarek R.L., 2003. Software User's Manual. EQ3/6, Version 8.0. Sandia National Laboratories–U.S. Department of Energy Report. pp. 376.
Zhang, J., Quay, P.D., Wilbur, D.O., 1995a. Carbon isotope fractionation during gas-water exchange and dissolution of CO_2. Geochimica Cosmochimca Acta 59, 107–114.
Zhang, J., Takahashi, K., Wushiki, H., Yabuki, S., Xiong, J.-M., Masuda, A., 1995b. Water geochemistry of the rivers around the Taklimakan Desert (NW China): crustal weathering and evaporation processes in arid land. Chemical Geology 119, 225–237.